

The Unique Type Ia Supernova 2000cx in NGC 524

Weidong Li¹, Alexei V. Filippenko¹, Elinor Gates², Ryan Chornock¹, Avishay Gal-Yam^{3,4},
Eran O. Ofek³, Douglas C. Leonard⁵, Maryam Modjaz¹, R. Michael Rich⁶, Adam G.
Riess⁷, and Richard R. Treffers¹

Email: wli@astro.berkeley.edu, alex@astro.berkeley.edu, egates@ucolick.org

Received _____; accepted _____

arXiv:astro-ph/0107318v1 17 Jul 2001

¹Department of Astronomy, University of California, Berkeley, CA 94720-3411.

²Lick Observatory, PO Box 82, Mount Hamilton, CA 95140.

³School of Physics and Astronomy, and the Wise Observatory, Tel Aviv University, Israel.

⁴Colton Fellow.

⁵Five College Astronomy Department, University of Massachusetts, Amherst, MA 01003-9305.

⁶Department of Physics and Astronomy, University of California, Los Angeles, CA 90095-1562.

⁷Space Telescope Science Institute, 3700 San Martin Drive, Baltimore, MD 21218.

ABSTRACT

We present extensive photometric and spectroscopic observations of the Type Ia supernova (SN Ia) 2000cx in the S0 galaxy NGC 524, which reveal it to be peculiar. Photometrically, SN 2000cx is different from all known SNe Ia, and its light curves cannot be fit well by the fitting techniques currently available. There is an apparent asymmetry in the B -band peak, in which the premaximum brightening is relatively fast (similar to that of the normal SN 1994D), but the postmaximum decline is relatively slow (similar to that of the overluminous SN 1991T). The color evolution of SN 2000cx is also peculiar: the $(B - V)_0$ color has a unique plateau phase and the $(V - R)_0$ and $(V - I)_0$ colors are very blue.

Although the premaximum spectra of SN 2000cx are similar to those of SN 1991T-like objects (with weak Si II lines), its overall spectral evolution is quite different. The Si II lines that emerged near maximum B -band brightness stay strong in SN 2000cx until about three weeks past maximum. The change in the excitation stages of iron-peak elements is slow. Both the iron-peak and the intermediate-mass elements are found to be moving at very high expansion velocities in the ejecta of SN 2000cx.

We discuss theoretical models for SN 2000cx. SN 2000cx may be an overluminous object like SN 1991T, but with a larger yield of ^{56}Ni and a higher kinetic energy in the ejecta. We also briefly discuss the implications of our observations for the luminosity vs. light-curve width relation.

Subject headings: supernovae: general – supernovae: individual (SN 2000cx, SN 1991T)

1. INTRODUCTION

Studies of high-redshift SNe Ia have revealed a surprising cosmological result, that the expansion of the Universe is presently accelerating due to a nonzero cosmological constant (e.g., Riess et al. 1998a, 2001; Perlmutter et al. 1999). This result, however, is based on the assumption that there are no significant differences between SNe Ia at high redshift and their low-redshift counterparts. Although this assumption is supported to first order by comparisons of the photometric and spectroscopic properties of SNe Ia at high and low redshifts (e.g., Riess et al. 1998a, 2000; Coil et al. 2000), there is also some evidence for differences between SNe Ia at different redshifts (e.g., Riess et al. 1999; Falco et al. 1999; Aldering, Knop, & Nugent 2000; Howell, Wang, & Wheeler 2000; Li et al. 2001). It is thus important to verify this assumption by further observations of high-redshift and nearby SNe Ia.

High-quality observations of nearby SNe Ia provide valuable information about their progenitor evolution and the relevant physics. Analyses of samples of well-observed nearby SN Ia enable observers to study the differences among SNe Ia, empirical correlations, and possible environmental effects (e.g., Hamuy et al. 2000). It is thus important to expand the sample of well-observed nearby SNe Ia.

SN 2000cx in the S0 galaxy NGC 524 was discovered and confirmed by the Lick Observatory Supernova Search (LOSS; Treffers et al. 1997; Li et al. 2000; Filippenko et al. 2001) with the 0.76 m Katzman Automatic Imaging Telescope (KAIT) in unfiltered images taken on 2000 July 17.5 and 18.4 UT (Yu, Modjaz, & Li 2000; UT dates are used throughout this paper). A low-resolution optical spectrum obtained with the Lick Observatory 1-m Nickel telescope on July 23 (Chornock et al. 2000) identified the event as a peculiar SN 1991T-like type Ia, with prominent Fe III absorption troughs near 4300 Å and 4900 Å but weak Si II at 6150 Å. Yu, Modjaz, & Li (2000) measured an accurate position for SN 2000cx as $\alpha = 1^{\text{h}}24^{\text{m}}46^{\text{s}}.15$, $\delta = +9^{\circ}30'30''.9$ (equinox J2000.0), which is $23''.0$ west and $109''.3$ south of the nucleus of NGC 524. The SN was at magnitude 14.5 (unfiltered) at discovery, and subsequently became the brightest SN of the year 2000.

Shortly after the discovery of SN 2000cx, a follow-up program of multicolor photometry and spectroscopy was established at Lick Observatory. Photometry of SN 2000cx was also gathered at the Wise Observatory (WO) in Israel. This paper presents the results from these campaigns and is organized as follows. Section 2 contains a description of the observations and analysis of the photometry, including our methods of performing photometry, our calibration of the measurements onto the standard Johnson-Cousins system, our resulting multicolor light curves, and our comparisons between the light curves and color curves of SN 2000cx and those of other SNe Ia. Section 3 contains a description of the spectral observations and analysis. The good temporal coverage of the spectral observations enables us to monitor the evolution of many features. We also undertake a thorough comparison between the spectra of SN 2000cx and those of other SNe Ia. We discuss the implications of our observations in §4 and summarize our conclusions in §5.

2. PHOTOMETRY

2.1. Observations and Data Reduction

Broadband *UBVRI* images of SN 2000cx were obtained using an Apogee AP7 CCD camera with KAIT, but only the *BVRI* observations are reported in this paper. (The *U*-band data will be combined with observations of other SNe Ia and reported in a future paper.) The Apogee camera has a back-illuminated SITe 512×512 pixel CCD chip with UV2AR coating to boost the blue response. At the $f/8.2$ Cassegrain focus of KAIT, the $24 \mu\text{m}$ pixel of the chip yields a scale of $0''.8 \text{ pixel}^{-1}$, making the total field of view of the camera $6'.7 \times 6'.7$. The typical seeing at KAIT is around $3''$ full width at half maximum (FWHM), so the CCD images are well sampled.

The WO images of SN 2000cx were obtained with the Wise 1-m telescope in the $f/7$ configuration, as part of the WO queue-observing program. The CCD camera with the back-illuminated 1024×1024 pixel Tektronix chip was used in unbinned mode. With a pixel scale of about $0''.7 \text{ pixel}^{-1}$, the total field of view was $\sim 12' \times 12'$. The typical images have $\text{FWHM} \approx 2''.5$ and thus are also well sampled.

The bias and dark-current subtraction with subsequent twilight-sky flatfielding were accomplished automatically at each of the telescopes. Significant fringing in the I -band KAIT images could not be completely removed, probably because the near-infrared sky lines vary in brightness with time. No detectable fringing is seen in the WO images. The implication of the fringing for the photometry will be discussed in more detail later (§2.2).

Figure 1 shows a KAIT V -band image taken on 2000 July 25 with SN 2000cx and four local standard stars marked. Absolute calibration of the field was done with KAIT on 2000 September 5, 25, and 26 by observing Landolt (1992) standard stars at different airmasses throughout the photometric nights. Instrumental magnitudes for the standard stars were measured using aperture photometry with the IRAF⁸ DAOPHOT package (Stetson 1987) and then used to determine transformation coefficients to the standard system of Johnson et al. (1966, for BV) and Cousins (1981, for RI). The derived transformation coefficients and color terms were then used to calibrate the sequence of four local standard stars in the SN 2000cx field. The magnitudes of those four stars and the associated uncertainties derived by averaging over the three photometric nights are listed in Table 1. The field of SN 2000cx was not calibrated at WO, so the WO images were also reduced against these local standard stars.

We used the point-spread-function (PSF) fitting method (Stetson 1987) to perform differential photometry of SN 2000cx relative to the comparison stars. Although SN 2000cx is at a fortunate position (far from the nucleus of the host galaxy, with a faint and smoothly varying background) and simple aperture photometry might suffice, we chose to use PSF fitting for the following two reasons. (1) PSF fitting usually gives more accurate measurements than aperture photometry for objects projected upon slightly more complex regions. It also has the advantage of creating an image with all the measured objects subtracted, which can serve as an indicator of the quality of the magnitude measurements

⁸IRAF (Image Reduction and Analysis Facility) is distributed by the National Optical Astronomy Observatories, which are operated by the Association of Universities for Research in Astronomy, Inc., under cooperative agreement with the National Science Foundation.

of the comparison stars and the SN. (2) PSF fitting handles the fringing in the I -band KAIT images better than aperture photometry does, especially at late times when the SN was rather faint.

Before the photometry measurements were initiated, cosmic rays were carefully removed from all the images, and dark-current residuals were manually eliminated from the KAIT images. This latter step is taken because the KAIT CCD camera is cooled thermoelectrically rather than with liquid nitrogen, so the temperature of the camera is not very stable and dark current is not always cleanly subtracted from the images. The resulting low-level dark-current residual varies from image to image and must be removed manually by adding or subtracting a few percent of the long-exposure dark-current image. The uncertainties introduced by the manual scaling and removing of the dark current have only negligible effects on the magnitude measurements of the high-contrast SN and the local standard stars. The WO CCD camera is cooled by liquid nitrogen, and there is no dark-current residual problem in the images.

The PSF for each image was determined with DAOPHOT using Stars 1, 3, and 4 (Star 2 is a bit too close to the host galaxy), which are bright and well-isolated. To increase the signal-to-noise ratio of the differential photometry, we used only the inner core (with a radius comparable to the FWHM) of SN 2000cx and the local standard stars to fit the PSF. The sky backgrounds of the stars were measured using an annulus with an inner radius of 20 pixels ($16''$ in the KAIT images and $14''$ in the WO images) and an outer radius of 25

Table 1. Photometry of comparison stars

ID	V	$(B - V)$	$(V - R)$	$(V - I)$
1	12.555(007)	0.586(009)	0.378(006)	0.760(007)
2	13.506(008)	0.797(009)	0.477(006)	0.921(008)
3	12.800(007)	0.696(008)	0.406(007)	0.794(007)
4	14.540(018)	0.829(008)	0.459(010)	0.887(009)

Note: uncertainties are indicated in parentheses.

pixels (20" in the KAIT images and 17".5 in the WO images).

The standard Johnson-Cousins $BVRI$ magnitudes of SN 2000cx were obtained by doing differential photometry between the instrumental magnitudes of the SN and those of the four local standard stars. The color terms involved in this transformation are -0.06 , 0.04 , 0.08 , and -0.01 for the KAIT B , V , R , and I filters, respectively. Notice that these color terms are quite different from those used by Modjaz et al. (2000) for the KAIT data on SN 1998de, especially in the R band. This is caused by our installation of a new set of filters for KAIT in 1999, whose transmissivities were made to match those defined by Bessell (1990) for the Johnson-Cousins $UBVRI$ photometric system. The color terms for the WO 1-m B , V , R , and I filters are -0.11 , -0.02 , -0.02 , and -0.04 , respectively.

Table 2. KAIT photometry of SN 2000cx

JD – 2450000	<i>B</i> (mag)	<i>V</i> (mag)	<i>R</i> (mag)	<i>I</i> (mag)
1743.97	14.41(03)	14.23(04)	14.17(03)	14.25(03)
1744.96	14.17(02)	14.00(02)	13.97(03)	14.10(03)
1746.00	13.95(02)	13.80(02)	13.78(02)	13.88(02)
1746.99	13.79(02)	13.65(02)	13.68(04)	13.78(04)
1749.95	13.48(05)	13.33(08)	13.35(09)	–
1750.95	13.45(02)	13.34(02)	13.39(03)	13.63(02)
1752.96	13.44(02)	13.27(02)	13.36(02)	13.72(02)
1753.96	13.45(02)	13.27(02)	13.36(02)	13.77(02)
1754.96	13.49(02)	13.25(02)	13.37(02)	13.81(02)
1756.92	13.58(02)	13.30(02)	13.40(02)	13.88(02)
1757.96	13.65(02)	13.31(02)	13.47(03)	14.03(04)
1758.96	13.73(02)	13.38(02)	13.55(02)	14.08(02)
1759.96	13.77(03)	13.42(02)	13.66(03)	14.13(03)
1760.99	13.84(03)	13.46(02)	13.69(02)	14.27(03)
1761.99	13.97(02)	13.56(02)	13.82(03)	14.44(05)
1762.99	14.02(02)	13.62(02)	13.94(02)	14.52(04)
1764.94	14.16(02)	13.78(02)	14.14(03)	14.64(06)
1766.94	14.32(02)	13.91(02)	14.24(04)	14.72(05)
1768.98	14.54(03)	14.07(02)	14.32(04)	14.72(03)
1770.92	14.72(03)	14.16(02)	14.36(03)	14.66(03)
1772.92	14.94(02)	14.27(03)	14.35(04)	14.58(03)
1778.93	15.64(03)	14.77(02)	14.54(03)	14.49(04)
1780.89	15.85(03)	14.93(02)	14.70(04)	14.57(06)
1783.92	16.10(03)	15.22(03)	14.90(04)	14.76(03)
1789.96	16.43(06)	15.51(05)	15.24(06)	15.28(13)
1791.88	16.48(02)	15.59(03)	15.33(02)	15.36(02)
1792.80	16.50(03)	15.62(03)	15.37(03)	15.38(03)
1794.90	16.56(03)	15.72(03)	15.47(03)	15.54(03)
1796.86	16.59(03)	15.78(02)	15.52(04)	15.64(03)
1805.92	16.79(04)	16.10(03)	15.89(03)	16.17(05)
1810.95	16.93(03)	16.27(02)	16.09(04)	–
1812.86	16.92(03)	16.33(03)	16.19(05)	16.48(05)
1813.80	16.95(03)	16.33(03)	16.15(03)	16.47(04)
1817.90	17.03(04)	16.48(03)	16.32(03)	16.75(04)
1821.88	17.08(03)	16.63(03)	16.47(04)	16.94(05)
1825.84	17.18(04)	16.71(03)	16.59(03)	17.09(05)
1832.87	17.35(12)	–	–	–
1836.82	17.37(04)	16.99(03)	16.96(03)	17.48(10)
1840.87	17.49(05)	17.14(03)	17.12(06)	17.84(16)
1845.88	17.60(10)	17.29(09)	17.36(09)	–
1849.87	17.85(28)	17.31(13)	17.46(08)	18.32(24)
1853.82	17.73(06)	17.50(04)	17.49(04)	18.31(09)
1861.82	17.85(08)	17.67(08)	17.71(09)	18.54(15)
1865.79	18.00(09)	17.74(07)	17.84(06)	18.49(10)
1873.70	18.06(05)	17.89(05)	18.03(05)	18.77(11)
1881.67	18.23(05)	18.03(05)	18.18(06)	19.15(16)
1889.65	18.36(10)	18.17(11)	–	19.06(17)
1897.67	18.59(08)	–	18.80(14)	–
1905.58	18.73(08)	18.54(07)	19.00(13)	–

Our final *BVRI* measurements of SN 2000cx are listed in Table 2 for KAIT and Table 3 for the WO telescope. Uncertainties for the measurements were estimated by combining in quadrature the errors given by the photometry routines in DAOPHOT with those introduced by the transformation of instrumental magnitudes onto the standard system.

2.2. Optical Light Curves

2.2.1. Overall Results

Figure 2 displays our *BVRI* light curves of SN 2000cx. The KAIT data points are shown with open circles and the WO ones with solid circles. For most of the points the uncertainties are smaller than the plotted symbols. The overall agreement between the measurements from the two telescopes is excellent. When KAIT data points are linearly interpolated to estimate photometry at the epochs of the WO observations, the difference between the KAIT and the WO photometry is usually less than 0.04 mag. However, there seem to be some differences in the *I* band, in particular between JD 2,451,765 and 2,451,780 and after JD 2,451,840. The SN was quite bright in the *I* band (<14.8 mag) between JD 2,451,765 and 2,451,780, so the offset between the measurements, with WO being brighter by about 0.1 mag, may be caused by the differences in the CCD infrared response and the *I*-band filter transmission curve of the two systems (i.e., even after the transformation onto the standard system using proper color terms, as discussed below). The SN became fainter than 17.5 mag in the *I* band after JD 2,451,840, and the fringing in the *I*-band KAIT images makes it difficult to obtain accurate magnitudes even with PSF fitting. Compared with the WO measurements, the KAIT data show larger fluctuations in the light curve. For this reason, we consider the WO measurements for the late-time *I*-band photometry to be more representative of SN 2000cx than the KAIT ones.

Kevin Krisciunas (2001, private communication) made available to us the photometry of SN 2000cx obtained at the Apache Point Observatory (APO) and the Manastash Ridge Observatory (MRO). A comparison between the KAIT and the APO/MRO photometry of SN 2000cx indicates that they agree with each other to 0.02 mag except in the *I* band,

Table 3. Wise Observatory photometry of SN 2000cx

JD – 2450000	<i>B</i> (mag)	<i>V</i> (mag)	<i>R</i> (mag)	<i>I</i> (mag)
1753.53	13.42(02)	13.25(02)	13.34(03)	13.76(02)
1754.56	13.44(03)	13.23(02)	13.32(02)	13.78(02)
1755.48	13.49(04)	13.23(03)	13.35(03)	13.81(04)
1760.44	13.81(02)	13.43(02)	13.62(03)	14.20(03)
1762.51	13.94(02)	13.59(02)	13.85(03)	14.39(02)
1767.47	14.36(02)	13.96(03)	14.20(03)	14.60(03)
1774.46	15.11(05)	14.40(04)	14.35(04)	14.44(05)
1777.53	–	14.62(05)	14.47(03)	14.41(04)
1778.56	15.61(03)	14.75(05)	14.51(03)	14.39(03)
1794.33	16.53(05)	15.67(03)	15.45(04)	15.42(03)
1795.48	16.62(03)	15.75(02)	15.51(03)	15.52(03)
1801.38	16.76(08)	15.99(05)	15.75(05)	15.89(05)
1809.44	16.87(03)	16.23(03)	16.03(03)	16.22(03)
1810.45	16.88(03)	16.22(03)	16.05(04)	16.31(04)
1811.34	16.93(03)	16.25(03)	16.09(03)	16.42(05)
1819.27	17.12(06)	16.53(04)	16.39(03)	16.71(05)
1821.42	17.12(03)	16.60(03)	16.45(03)	–
1822.33	17.15(04)	16.60(03)	16.49(03)	16.92(05)
1837.32	17.42(05)	17.06(04)	17.00(05)	17.42(12)
1842.24	17.47(05)	17.17(04)	17.25(05)	17.78(25)
1845.27	17.53(04)	17.30(03)	17.26(03)	17.63(05)
1846.27	17.54(04)	17.26(02)	17.26(05)	17.89(04)
1856.29	–	17.52(04)	17.68(05)	18.04(09)
1864.28	–	17.71(03)	17.78(04)	18.37(06)
1865.32	–	17.75(03)	17.82(03)	18.44(05)
1870.30	–	17.87(03)	17.98(03)	18.50(05)
1878.33	–	18.02(03)	18.18(03)	18.86(10)

Note: uncertainties are indicated in parentheses.

where the APO/MRO measurements are systematically brighter by about 0.05 mag.

Suntzeff (2000) found that there was a systematic difference of about 0.07 mag in the BV passbands between two data sets of SN 1998bu obtained with two telescopes at Cerro Tololo Inter-American Observatory (CTIO), and cautioned the need for photometrists to correct their measurements to a standard filter transmission curve using spectrophotometry. We found that for the case of SN 2000cx, the BVR measurements from different sources agree with each other quite well, probably due to similar filter transmission and CCD quantum efficiency in those passbands at different telescopes. Different CCD chips usually have somewhat different infrared responses, and the I -band filter transmission curves are quite diverse, so it is not surprising that there are systematic differences among the I -band data sets of SN 2000cx. In any case, it seems that if a telescope has non-standard Johnson-Cousins filters, or if the CCD camera used for photometry has poor quantum efficiencies in certain passbands, it may be necessary to follow the suggestion by Suntzeff (2000) to correct the photometry using spectrophotometry, in a manner similar to K -corrections (e.g., Jha et al. 1999).

Here, and in all subsequent discussions and figures, the KAIT and the WO datasets of SN 2000cx are combined and discussed together. Also defined here is the variable t , which is the time since maximum brightness in the B band ($JD = 2451752.2$; see discussions below).

The date and the magnitude of the peak in each passband are listed in Table 4; they were determined by fitting different spline functions and polynomials to the $BVRI$ light curves around maximum brightness. Since we have nearly nightly observations of SN

Table 4. Photometric information on SN 2000cx

Filter	B	V	R	I
UT of max.	Jul 26.7 \pm 0.1	Jul 28.8 \pm 0.1	Jul 28.1 \pm 0.1	Jul 25.1 \pm 0.5
Julian Date of max.	2451752.2 \pm 0.1	2451754.3 \pm 0.1	245173.6 \pm 0.1	2451750.6 \pm 0.5
Magnitude at max.	13.43 \pm 0.03	13.25 \pm 0.03	13.37 \pm 0.04	13.62 \pm 0.04
Δm_{15}	0.93 \pm 0.04	0.82 \pm 0.05	0.94 \pm 0.05	1.06 \pm 0.06

2000cx from $t = -8$ to 20 days, the measurements from different fitting methods are quite consistent, yielding comparatively small uncertainties for them. Also listed in Table 4 are the Δm_{15} values for all the passbands. In accordance with Phillips (1993), $\Delta m_{15}(X)$ is defined as the decline (in magnitudes) during the first 15 days after maximum brightness in the passband X . As pointed out by Phillips (1993) and Hamuy et al. (1996a), these Δm_{15} values, especially $\Delta m_{15}(B)$, are good indicators of the luminosities of SNe Ia in the sense that a SN Ia with a smaller Δm_{15} value (also called a “slow decliner”) is more luminous than a faster decliner. This light-curve shape and luminosity correlation is often referred as the luminosity – $\Delta m_{15}(B)$ or the luminosity vs. light-curve width relation for SNe Ia.

In Figures 3, 4, 5, and 6, we compare the light curves of SN 2000cx with those of several other well-observed SNe Ia representing the diversity of SN Ia light curves: SN 1991T [$\Delta m_{15}(B) = 0.95 \pm 0.05$, Lira et al. 1998] as an example of an overluminous SN Ia; SN 1992bc [$\Delta m_{15}(B) = 0.87 \pm 0.05$, Hamuy et al. 1996b], SN 1992al [$\Delta m_{15}(B) = 1.11 \pm 0.05$, Hamuy et al. 1996b], and SN 1994D [$\Delta m_{15}(B) = 1.31 \pm 0.08$, Richmond et al. 1995] as examples of normal SNe Ia with different decline speeds in their light curves; and SN 1991bg [$\Delta m_{15}(B) = 1.93 \pm 0.08$, Filippenko et al. 1992a; Leibundgut et al. 1993] as an example of a subluminous SN Ia. All light curves are shifted in time and peak magnitude to match those of SN 2000cx with the time zero-point being the date of maximum light in the B band.

2.2.2. B Band

The B -band light curve of SN 2000cx (Figure 3) shows a peculiar evolution, unlike that of any other SN in the comparison. Before maximum brightness, SN 2000cx brightens much faster than SN 1991T, although its spectra show strong similarity to those of SN 1991T at this time (see §3 for more details of spectral comparisons). In fact, the rise of SN 2000cx is just like that of SN 1994D, whose spectra show apparent differences from those of SN 2000cx. Thus, the premaximum brightening of SN 2000cx provides a counterexample to the correlation between spectroscopic peculiarity and light-curve behavior of SNe Ia (Nugent et

al. 1995; Riess et al. 1998b).

The light curve of SN 2000cx follows that of SN 1994D until $t = 6$ days, but then it has a transition phase where the decline slows down (more easily seen in the inset of Figure 3) and changes to follow the light curve of SN 1991T from $t = 15$ to 22 days. Because of this transition phase, SN 2000cx has a $\Delta m_{15}(B)$ value of 0.93 ± 0.04 mag, very similar to that of SN 1991T (0.95 ± 0.05 mag). There is an apparent asymmetry in the rising and declining parts of the light curve for SN 2000cx, which might challenge the light-curve fitting techniques currently available for SNe Ia. For example, both the “stretch method” (Perlmutter et al. 1997) and the multicolor light-curve shape method (hereafter MLCS; Riess, Press, & Kirshner 1996) require all SNe Ia to constitute one family of well-behaved light curves. A similar, but less apparent asymmetry can be seen in the light curve of SN 1992bc (Figure 3). These asymmetries indicate that $\Delta m_{15}(B)$ may not be the only parameter characterizing the width of light curves of SNe Ia, and raise the question of whether SN Ia luminosities are correlated more with their $\Delta m_{15}(B)$ values or their light-curve widths.

There seems to be another transition between $t = 22$ and 30 days, during which time SN 2000cx declines faster (0.11 mag day $^{-1}$) than SN 1991T (0.09 mag day $^{-1}$), SN 1992bc (0.09 mag day $^{-1}$), and SN 1992al (0.10 mag day $^{-1}$). By $t = 30$ days, SN 2000cx begins to follow SN 1992al and continues until $t = 60$ days. At late times all SNe Ia in Figure 3 show a linear decline, with the decline rate measured in mag (100 days) $^{-1}$ sorted from the slowest to the fastest as follows: SN 1991T, 1.41; SN 1992bc, 1.49; SN 1992al, 1.54; SN 1994D, 1.77; SN 2000cx, 1.92; and SN 1991bg, 2.35. SN 2000cx has the second fastest decline rate.

2.2.3. *V Band*

The *V*-band light curve of SN 2000cx is shown in Figure 4. SN 2000cx behaves like SN 1994D until $t = 4$ days, and then evolves in a manner between SN 1992al and SN 1994D until $t = 30$ days. The excellent temporal coverage and high accuracy of the SN 2000cx photometry reveal a “shoulder” phase at $t = 16$ to 30 days. Considering the peculiar

photometric evolution of SN 2000cx, however, this shoulder phase may be unique to SN 2000cx and not common for all SNe Ia. After $t = 30$ days the light curve of SN 2000cx falls below that of SN 1994D, and joins that of SN 1991bg. It is remarkable that despite the huge difference in the light-curve shapes between SN 2000cx and SN 1991bg around peak brightness, the two SNe have a very similar total decline in the first 40 days after peak (2.45 mag for SN 2000cx and 2.47 mag for SN 1991bg).

Between $t = 50$ and 100 days all SNe show a linear decline, with the decline rates in $\text{mag (100 days)}^{-1}$ measured as follows: SN 1991T, 2.29; SN 1992bc, 2.47; SN 1992al, 2.63; SN 1994D, 2.74; SN 2000cx, 2.82; and SN 1991bg, 3.33. SN 2000cx again shows a faster decline than most of the SNe, second only to SN 1991bg.

The late-time V -band light curve of SN 2000cx ($t > 100$ days) is well observed. It seems that $t = 110$ days is a bending point for SN 2000cx, where the decline rate changes from $2.82 \text{ mag (100 days)}^{-1}$ to $1.95 \text{ mag (100 days)}^{-1}$. This bending point, however, is much less dramatic than the one at $t \approx 35$ days, and an alternative view is that the decline rate changes gradually over time. A change in the late-time decline rate is also found for SN 1991T (Lira et al. 1998) and SN 1991bg (Turatto et al. 1996), so it may be common in SNe Ia.

There is a general consensus that the late-time light curves of SNe Ia are powered by the radioactive decay energy of ^{56}Co to ^{56}Fe . Milne, The, & Leising (2001) used Monte Carlo algorithms to simulate the interactions of the products from this decay, γ -ray photons and positrons, and confirmed that the late-time light curves of SNe Ia can be explained with energy deposition from those γ -ray photons and positrons only if substantial positrons escape from the magnetic field of the ejecta. They also suggested that at late times ($t > 40$ days), the V -band flux constitutes a constant fraction ($\sim 25\%$) of, and thus scales as, the bolometric luminosity of a SN Ia. For SN 2000cx, the latest (and smallest) decline rate of $1.95 \text{ mag (100 days)}^{-1}$ in the V band (and thus in bolometric luminosity) is still steeper than that expected from the ^{56}Co to ^{56}Fe decay with instantaneous deposition of all decay energy [$0.98 \text{ mag (100 days)}^{-1}$], suggesting that the γ -ray photon and positron transport are indeed important at those late times.

2.2.4. *R Band*

The *R*-band light curve comparison is presented in Figure 5. SN 2000cx shows an evolution similar to that of SN 1994D, especially before $t = 0$ day and at $t = 30 - 70$ days. However, there are apparent differences between the two SNe from $t = 0$ to 30 days. As can be seen more clearly in the inset of Figure 5, SN 2000cx has a slower decline rate, but a larger overall decline after peak than SN 1994D does. The plateau phase begins at $t = 12$ days for SN 1994D, while it begins at $t = 16$ days for SN 2000cx. Unfortunately, there are no data available for SN 1994D after $t = 70$ days, so it is unclear whether the late-time evolution of SN 2000cx and SN 1994D is similar. The late-time photometry of SN 2000cx indicates that there may be a bending point at $t \approx 100$ days, but the changes in the decline rate may be gradual.

2.2.5. *I Band*

Figure 6 shows the *I*-band light curves of the SNe. SN 2000cx behaves like SN 1994D before $t = 7$ days, but then it declines faster and more than SN 1994D. The minimum of the “dip” between the two peaks of the *I*-band light curves occurs at about 0.6 mag below peak at $t \approx 10$ days for SN 1994D, while it occurs at about 1.1 mag below peak at $t \approx 14$ days for SN 2000cx. SN 2000cx has the most prominent “dip” among all the SNe Ia in the comparison. Pinto & Eastman (2000) examined the nature of the opacity and radiation transport in SNe Ia, and explored the reasons for those secondary maxima in the *I* band. They found that several weeks after maximum brightness, the ionization in regions of trapped radiation falls to include significant amounts of singly ionized species (Ca II, Fe II, and Co II) that can emit strongly in the near infrared. As a result, there is a decrease in the flux mean opacity, which reduces the diffusion time, allows the reservoir of trapped radiation to escape more rapidly, and leads to an increase in the luminosity. The more prominent “dip” and fainter secondary peak of SN 2000cx may thus indicate a slower evolution in the ionization stages of the species, which is consistent with the spectral evolution of SN 2000cx discussed in §3.

All SNe in Figure 6 show a linear decline after their second peak, with the decline rates in mag (100 days)⁻¹ measured as follows: SN 1992bc, 3.51; SN 1991bg, 3.66; SN 1992al, 3.78; SN 1991T, 4.05; SN 1994D, 4.71; and SN 2000cx, 4.79. SN 2000cx thus has the fastest decline rate after the second peak among all the SNe Ia in the comparison. The decline rate of SN 2000cx seems to change at $t \approx 100$ days, though the large scatter in the late-time photometry prevents us from making a definitive conclusion.

In summary, the light curves of SN 2000cx differ from those of all known SNe Ia. The closest match seems to be those of SN 1994D, especially in the R and I bands, but there remain significant differences between them. The “metamorphosis” in the B band (i.e., SN 2000cx looks like SNe 1994D, 1991T, and 1992al at different epochs) is puzzling, as are the large postmaximum decline in the V band and the secondary maximum evolution in the R and I bands.

2.3. Optical Color Curves

Strong host-galaxy reddening is not expected for SN 2000cx, since NGC 524 is an early-type galaxy of Hubble type S0. Moreover, SN 2000cx is located about 2' southwest of the nucleus (Figure 1) where no significant contamination is expected. Another argument against the presence of substantial host-galaxy reddening is that the spectra of SN 2000cx do not show signs of narrow interstellar Na I D absorption at the expected position (5940 Å). In most of the spectra, however, there is an apparent absorption feature at about 5890 Å (with equivalent width 1.1 ± 0.4 Å) caused by interstellar Na I within the Milky Way, indicating the existence of Galactic reddening toward SN 2000cx. Using the full-sky maps of dust infrared emission of Schlegel, Finkbeiner, & Davis (1998), we derive a Galactic reddening of $E(B - V) = 0.08$ mag for SN 2000cx. In subsequent discussions, we assume no host-galaxy extinction and use $E(B - V) = 0.08$ mag as the adopted total reddening for SN 2000cx.

In Figures 7, 8, and 9, we present the intrinsic optical color curves of SN 2000cx [$(B - V)_0$, $(V - R)_0$, and $(V - I)_0$], together with color curves of several other SNe

Ia (1991T, 1992bc, 1992al, and 1994D) for comparison. In order to calculate the color excess for the R and I passbands we adopt the standard reddening-law parameterization, $E(V - R)/E(B - V) = 0.78$ and $E(V - I)/E(B - V) = 1.60$ (Savage & Mathis 1979). The reddenings adopted for the comparison SNe are $E(B - V) = 0.13$ mag for SN 1991T (Phillips et al. 1992), 0.02 mag for SN 1992bc (Phillips et al. 1999), 0.04 mag for SN 1992al (Phillips et al. 1999), and 0.04 mag for SN 1994D (Richmond et al. 1995).

The color evolution of SN 2000cx is peculiar. The $(B - V)_0$ color curve in Figure 7 shows that SN 2000cx has $(B - V)_0 = 0.10$ mag at $t = -8$ days, the reddest of all the SNe in the comparison sample. In fact, SN 2000cx has the reddest color among all the SNe in Figure 7 until $t \approx 10$ days. SN 2000cx has a unique phase of nearly constant color at $(B - V)_0 \approx 0.3$ mag at $t = 6 - 15$ days, which corresponds to the transition phase seen in the B -band light curve (Figure 3). Because of this unusual plateau phase, by $t = 15$ days SN 2000cx has the second *bluest* color (exceeded only by SN 1992bc) among all the SNe in Figure 7. All these SNe show an approximately linear increase in color between $t = 15$ and 30 days, though the slopes differ somewhat (SN 2000cx has the smallest one).

Lira (1995) found that the $(B - V)$ colors of several apparently unreddened SNe Ia evolved in a nearly identical fashion from $t = 30$ to 90 days. This property, which was further discussed by Phillips et al. (1999), is shown in Figure 7 as the “L–P law” (which stands for the “Lira-Phillips law”). Phillips et al. (1999) noted that individual SNe could display systematic residuals with respect to this fit and suggested an intrinsic dispersion of ~ 0.05 mag for the fit, which seems to be too small for the SNe in Figure 7: SNe 1991T and 1992al are ~ 0.1 mag redder than the fit. While the bad fit to SN 1991T could be caused by an incorrect estimate of its reddening, SN 1992al is an apparently unreddened SN Ia (Hamuy et al. 1996b; Phillips et al. 1999). The most disturbing case, however, is SN 2000cx, which shows a color ~ 0.2 mag *bluer* than the fit. Increasing the reddening to SN 2000cx will only make it intrinsically bluer, further deviating from the fit. Thus, although the L-P law provides an independent method to estimate the extinction toward SNe Ia, it should be used with caution for any individual SN.

The late-time $(B - V)_0$ evolution ($t > 90$ days) of SN 2000cx is well sampled. These

points, despite large uncertainties, suggest that SN 2000cx has a nearly constant color between $t = 90$ and 150 days. SN 1992bc also seems to have a nearly constant color from $t = 80$ to 110 days, while SN 1992al seems to have a linear decrease during this period. Hence, the late-time color evolution of SNe Ia seems to be diverse, although the current sample is too small to permit a definitive conclusion.

The $(V - R)_0$ color evolution of the SNe Ia is shown in Figure 8. SN 2000cx has the bluest color until $t = 25$ days. It has a linear decline in color at a rate of $0.014 \text{ mag day}^{-1}$ between $t = -8$ to 6 days, then switches to a faster decline at a rate of $0.030 \text{ mag day}^{-1}$ until $t = 12$ days. This faster decline phase also correlates with the transition phase in the B -band light curve and the plateau phase in the $(B - V)_0$ color evolution. The bluest color of SN 2000cx, $(V - R)_0 \approx -0.4 \text{ mag}$, occurs at $t \approx 12$ days. This color is about 0.2 mag bluer than that of SN 1994D and 0.35 mag bluer than that of SN 1992bc at the same epoch. There is a dramatic difference in the $(V - R)_0$ color evolution before $t = 20$ days between SN 2000cx and SN 1992bc: SN 1992bc shows a very flat evolution, while SN 2000cx develops a prominent “dip” during this time. It is thus interesting to notice that these two SNe share similar evolution from $t = 20$ to 30 days. At late times ($t > 30$ days), SN 2000cx shows a very normal $(V - R)_0$ color evolution compared to the other SNe Ia in Figure 8.

Figure 9 shows that SN 2000cx has the bluest $(V - I)_0$ color of all the SNe Ia in the comparison sample (except during $t = 20$ to 30 days, at which time SN 1992bc is bluer than SN 2000cx). From $t = -8$ to 10 days, SN 2000cx becomes progressively bluer by ~ 0.9 mag, about 0.3 mag more than the other SNe do. The $(V - I)_0$ color at $t = 10$ days is -1.0 mag, the bluest of all known SNe Ia. During the transition phase in the B -band light curve and the plateau phase in the $(B - V)_0$ color curve ($t = 6$ to 15 days), the $(V - I)_0$ color of SN 2000cx develops the bluest “dip.” All the SNe in Figure 9 show an approximately linear increase in color between $t = 10$ and 30 days, although SN 2000cx has the biggest slope (about $0.07 \text{ mag day}^{-1}$). SN 2000cx also has the bluest $(V - I)_0$ color at $t > 30$ days, during which time all the SNe show a linear decrease in color.

It is interesting to note that even though the premaximum brightening of SN 2000cx is exactly the same as that of SN 1994D in all $BVRI$ passbands, their colors are quite

different: SN 2000cx is redder by 0.1 mag in $(B - V)_0$, and bluer by 0.1 mag in $(V - R)_0$ and $(V - I)_0$, than SN 1994D. Thus color evolution of SNe Ia, if available, may reveal differences among SNe Ia that are otherwise hidden in their light-curve shapes.

In summary, the color evolution of SN 2000cx is peculiar. In $(B - V)_0$, the relatively red color at $t < 6$ days, the plateau phase between $t = 6$ and 15 days, and the blue late-time tail ($t > 30$ days) are unique. The very blue color at $t = 5$ to 20 days in $(V - R)_0$ and $(V - I)_0$, and the blue late-time tail ($t > 30$ days) in $(V - I)_0$, are also puzzling. In §3, we will investigate how the peculiarities in the light curves and color curves of SN 2000cx are correlated with its spectral evolution.

3. SPECTROSCOPY

3.1. General Results

Spectroscopic observations of SN 2000cx were conducted with the Lick Observatory 1-m Nickel telescope (hereafter L1) using its spectrograph, and with the Lick 3-m Shane telescope (hereafter L3) using the Kast spectrograph (Miller & Stone 1993). The journal of observations is given in Table 5.

All one-dimensional sky-subtracted spectra were extracted optimally (Horne 1986) in the usual manner, generally with a width of $\sim 10''$ along the slit. Each spectrum was wavelength and flux calibrated, and corrected for continuum atmospheric extinction and telluric absorption bands (Bessell 1999; Matheson 2000).

In general, the position angle of the slit was aligned along the parallactic angle for the L3 observations (except those in spectropolarimetric mode), so that the spectral shape does not suffer from differential light loss (Filippenko 1982). The L1 observations, on the other hand, were all obtained with a fixed angle of 0° at relatively large airmasses (1.7 to 2.2), making their continuum shape unreliable. Leonard (2001, his Figure 5.5) also found that the continuum shape at $\lambda \geq 5800 \text{ \AA}$ of some of the L1 spectra of SN 1999em suffered from a mysterious problem, whose symptom is that successive observations during the same

Table 5. Journal of spectroscopic observations of SN 2000cx

UT Date	t^a (day)	Tel. ^b	Range ^c (Å)	Air. ^d	Slit (arcsec)	Exp. (s)	Observer(s) ^e
2000-07-23	−3	L1	3801-7340	2.0	2.9	4×900	EG
2000-07-24	−2	L1	3769-6793	2.0	2.9	4×900	EG
2000-07-25	−1	L1	3769-7340	2.1	2.9	4×900	EG
2000-07-26	+0	L1	3819-7142	2.1	2.9	4×900	EG
2000-07-27	+1	L1	3769-7241	2.1	2.9	4×900	EG
2000-07-28	+2	L3	3323-9919	1.7	2.0	2×200	AF, RC
		L3p	4300-6900	1.4	3.0	4×1500	AF, RC
2000-08-01	+6	L3	3323-10193	1.1	2.0	2×300	MR
2000-08-02	+7	L3	3323-10400	1.1	2.0	2×300	MR
2000-08-03	+8	L1	3918-7390	2.1	2.9	3×1200	EG
2000-08-05	+10	L1	3918-7390	2.1	2.9	3×1200	EG
2000-08-07	+12	L1	3918-7390	2.1	2.9	3×1200	EG
2000-08-10	+15	L1	3918-7390	2.2	2.9	3×1200	EG
2000-08-15	+20	L1	3918-7390	2.0	2.9	3×1200	EG
2000-08-18	+23	L1	3918-7390	2.2	2.9	3×1200	EG
2000-08-20	+25	L1	3918-7390	1.9	2.9	3×1200	EG
2000-08-22	+27	L1	3918-7390	2.1	2.9	3×1200	EG
2000-08-24	+29	L1	3918-7390	1.8	2.9	3×1200	EG
2000-08-26	+31	L1	3918-7390	1.7	2.9	3×1200	EG
	+31	L3p	4300-6900	1.4	3.0	2×1500	DL, WL
						2×1800	
2000-08-27	+32	L3	3273-10365	1.1	2.0	450	AF, WL, DL
	+32	L3p	4300-6900	1.4	3.0	4×1500	AF, WL, DL
2000-09-06	+42	L3	3273-10365	1.1	2.0	700	AF, RC, WL
2000-09-26	+62	L3	3273-10316	1.1	2.0	1200	AF, RC, WL
2000-10-06	+72	L3	3273-10316	1.1	2.0	1800	AF, RC
2000-10-24	+90	L3	3273-10316	1.1	2.0	1800	AF, RC
2000-11-01	+98	L3	3273-9907	1.2	2.0	2×1800	AF, WL
2000-11-29	+126	L3	3273-10380	1.1	2.0	1800	AF, RC
2000-12-21	+148	L3	3273-10415	1.1	2.0	2700	AF, RC, MM

^aDays since B maximum brightness (JD = 2451572.2), rounded to the nearest day.

^bL1 = Lick 1-m/Nickel reflector + spectrograph; L3(p) = Lick 3-m/Shane reflector + Kast double spectrograph (“p” denotes polarimeter attached).

^cObserved wavelength range of spectrum.

^dAverage airmass of observations.

^eAF = Alex Filippenko; DL = Douglas Leonard; EG = Elinor Gates; MM = Maryam Modjaz; MR = Michael Rich; RC = Ryan Chornock; WL = Weidong Li.

night on a few nights showed large variations. This problem, however, is not present in the L1 data on SN 2000cx – the reductions show that successive observations are consistent with each other. Li et al. (2001, in preparation) show that the L1 data on SN Ia 1999by do not suffer from this problem either. Thus, the problem found by Leonard (2001) appears to be sporadic.

Besides normal spectroscopy, spectropolarimetry (range 4300 to 6900 Å) of SN 2000cx was obtained with L3 on three nights: 2000 July 28, August 26, and August 27. Preliminary analysis of the observations on 2000 July 28 (Leonard et al. 2001) indicates a continuum polarization of about 0.5%. A strong polarization modulation (about 0.3%) across the Si II λ 6355 line is found, implying significant polarization intrinsic to SN 2000cx itself, possibly resulting from an aspherical scattering atmosphere (e.g., Höflich 1991). Detailed results of the spectropolarimetry will be the topic of a future paper; here only the total-flux spectra are reported.

The spectral evolution of SN 2000cx from $t = -3$ to 148 days is shown in Figures 10 and 11. All spectra shown in this paper have been corrected for reddening and for the host-galaxy redshift. For SN 2000cx, we adopt a reddening of $E(B - V) = 0.08$ mag as discussed earlier, and a redshift of 2421 km s⁻¹ from NED⁹. With 29 spectra obtained from $t = -3$ to +148 days, SN 2000cx is one of the spectroscopically best-observed SNe Ia.

Our strategy for studying the spectral evolution of SN 2000cx is to use Figures 10 and 11 as a guide, and to conduct detailed comparisons between SN 2000cx and other SNe Ia at different epochs in Figures 12 through 17. The example of a normal SN Ia used in the comparison is SN 1994D (Patat et al. 1996; Filippenko 1997). Since the premaximum spectra of SN 2000cx are similar to those of SN 1991T, we include in the comparison SN 1991T (Filippenko et al. 1992b) and SN 1997br, another SN 1991T-like SN Ia (Li et al. 1999). The line identifications adopted here are taken from Kirshner et al. (1993), Jeffery

⁹NED (NASA/IPAC Extragalactic Database) is operated by the Jet Propulsion Laboratory, California Institute of Technology, under contract with the National Aeronautics and Space Administration.

et al. (1992), and Mazzali, Danziger, & Turatto (1995).

3.2. The First Three Weeks

The top spectrum in Figure 10 was obtained with L1 on 2000 July 23, 6 days after the discovery of SN 2000cx. Figure 12 shows a comparison of this spectrum with those of other SNe Ia at similar epochs ($t = -3$ days). The spectrum of SN 2000cx is similar to that of SN 1997br: Fe III $\lambda 4404$ and Fe III $\lambda 5129$ are the two major absorption lines, and the Si II $\lambda 6355$ line is much weaker than that of SN 1994D, with an asymmetric profile similar to that seen in SN 1997br. There seems to be some high-excitation Si III lines in the spectrum; Si III $\lambda 4560$ is weak but apparent, and the line at ~ 5500 Å marked with a “?” may be Si III $\lambda 5740$.

The overall continuum of SN 2000cx seems to be redder than those of SNe 1994D and 1997br. While this could be caused by the differential light loss for the L1 observations, it is confirmed by the concurrent red photometric $(B - V)_0$ values. A redder continuum, with a lower color temperature, is often regarded as being associated with a lower radiation temperature as well. Pinto & Eastman (2000), however, demonstrate that the observed spectral continuum shape (and thus the color temperature) may have less to do with close thermal coupling between the gas and the radiation field and more to do with the distribution of lines and branching ratios in the complex atomic physics of the iron group. In other words, the redder continuum of SN 2000cx does not necessarily mean that it has a cooler radiation field – it may be caused by different excitation conditions and/or distribution of the iron-peak elements. As discussed later, we favor the latter explanation.

One interesting feature of the SN 2000cx spectrum at $t = -3$ days is the narrow emission at about 4060 Å (marked by a “?” in Figure 11), which appears in the spectra of SN 2000cx until $t = 7$ days. It is often accompanied by another narrow emission line at about 3860 Å (see the $t = 2, 6,$ and 7 days spectra in Figure 10; also see Figure 12). The nature of those two narrow emission lines is not clear. While their wavelengths are coincident with those of H δ and H ζ blueshifted by about 3,000 km s⁻¹, the lack of other

hydrogen Balmer lines makes these identifications very unlikely. Perhaps the apparent “emission lines” are explained by a lack of absorption at these wavelengths.

From $t = -3$ to $+2$ days (Figure 10), Si II $\lambda 6355$ becomes progressively stronger. Fe III $\lambda 4404$ remains prominent, although its profile shows evolution during this time – the blue wing becomes steeper from $t = -3$ to -1 day, then flatter again to $t = 2$ days, while Si III $\lambda 4560$ at the red wing becomes weaker and vanishes at $t \approx 2$ days. The blue wing of Fe III $\lambda 5129$ seems to be contaminated by a strengthening absorption that is probably Si II $\lambda 5051$. The S II $\lambda 5468$ and S II $\lambda \lambda 5612, 5654$ lines also strengthen with time.

By $t = 2$ days, the spectrum of SN 2000cx looks almost normal, though a detailed comparison (Figure 13) shows that there are still noticeable differences. Neither SN 1991T nor SN 1997br have spectra at this epoch so they are not included in the comparison. The largest difference between SN 2000cx and SN 1994D at this epoch is the relatively weaker features for the intermediate-mass elements (Si II, Ca II, S II, and O I), and the relatively stronger Fe III $\lambda 4404$ and Fe III $\lambda 5129$ lines, in the spectrum of SN 2000cx. The two mysterious narrow emission lines discussed earlier are still present. There are also apparent differences in the spectral range from 7800 to 8400 Å – SN 1994D shows a strong Ca II IR triplet, while SN 2000cx shows four absorption wiggles. The two wiggles at the red side correspond to the Ca II IR triplet, but the two at the blue side do not have counterparts in the spectrum of SN 1994D. We have difficulty identifying these two wiggles at the blue side, but suspect that they may be part of the Ca II IR triplet absorption caused by some unique distribution of Ca in the ejecta of SN 2000cx. This identification, however, requires part of the Ca in the ejecta of SN 2000cx to have very high expansion velocity ($\geq 28,000$ km s⁻¹). Hatano et al. (1999) found evidence for very high expansion velocity for Ca II features in the spectra of SN 1994D, but at a much earlier phase ($t = -8$ days). They suggested that the lower-velocity matter represents freshly synthesized material, while the highest-velocity matter is likely to be primordial. Similar wiggles can be seen in the near-maximum spectrum of SN 1991T (Filippenko et al. 1992b), possibly in the data on SN 1997br (Li et al. 1999), and in other SN 1991T-like objects (Li et al. 2001, in preparation), but not in normal SNe Ia such as SN 1981B (Branch et al. 1983), SN 1989B (Wells et

al. 1994), and SN 1992A (Kirshner et al. 1993). It is unclear how the differences in the evolution of Ca II profiles are related to the models of SNe Ia.

Between $t = 6$ and 15 days, SN 2000cx experienced the transition phase in the B -band light curve, the plateau phase in the $(B - V)_0$ color curve, and the bluest color in the $(V - R)_0$ and $(V - I)_0$ evolution. Spectroscopically (Figure 10), it is puzzling how the $(B - V)_0$ color of SN 2000cx could be nearly constant during this period because there is apparent evolution in the spectra of SN 2000cx that corresponds to the broad BV passbands (3500 – 6500 Å), especially during $t = 10$ to 15 days. The S II $\lambda 5468$ and S II $\lambda\lambda 5612, 5654$ lines become progressively weaker and vanish at $t \approx 12$ days. The Na I D and Si II $\lambda 5972$ blend at ~ 5750 Å becomes much stronger and dominates the spectrum at $t = 15$ days. The Fe III $\lambda 5129$ line is also contaminated by Si II $\lambda 5051$. One possible explanation for the constant $(B - V)_0$ color is that the change in the features is compensated by a change in the continuum shape. While most changes in features happened in the V band (4800 – 6500 Å) and they tend to increase the $(B - V)_0$ color (because of fewer absorption lines in the V band), the continuum shape seems to become bluer from $t = 10$ to 15 days which reduces the $(B - V)_0$ color. These two opposite trends cancel out and result in a constant color in $(B - V)_0$. The blue continuum is also consistent with the very blue $(V - R)_0$ and $(V - I)_0$ color evolution during this time. Since the spectral features in the R band (5700 – 7500 Å) do not change significantly, the blue $(V - R)_0$ color is almost certainly caused by the blue continuum of the spectra. Unfortunately, our spectra do not cover the whole I band during this time, so it is unclear how the spectral features (in particular, the Ca II IR triplet) change in this spectral range (7300 – 9000 Å).

Also unique to SN 2000cx at this time is the persistence of strong, high-excitation Fe III and weak Fe II lines. The high-excitation Fe III lines are usually seen in the premaximum spectra of SN 1991T-like objects, but in the case of SN 2000cx, the Fe III $\lambda 4404$ is very strong at 4260 Å even in the $t = 15$ day spectrum (Figure 14). While it could be argued that this line may be the Fe II $\lambda 4555$ line at high expansion velocities, we dispute this identification for two reasons: (1) the good temporal coverage of the spectra of SN 2000cx from $t = -3$ to 15 days shows clearly that this line evolved from the Fe III $\lambda 4404$ line in

the $t = -3$ day spectrum; and (2) the Fe II $\lambda 4555$ line is seen to develop in the $t = 20$ day spectrum (Figure 15) at a more reasonable wavelength. A high expansion velocity of more than $20,000 \text{ km s}^{-1}$ is required to identify the absorption at 4260 \AA as the Fe II $\lambda 4555$ line, while the expansion velocity measured from the Fe II $\lambda 4555$ line at $t = 20$ days is only about $10,000 \text{ km s}^{-1}$. It is unlikely that the expansion velocity measured from the same line could change by more than $10,000 \text{ km s}^{-1}$ in just 5 days.

Other evidence for strong Fe III and weak Fe II lines in the spectra of SN 2000cx is the presence of Fe III $\lambda 5129$ and the absence of Fe II $\lambda 5169$ in the $t = 15$ day spectrum (Figure 14). The Fe II lines that usually contaminate Si II $\lambda 6355$ are also absent, even in the $t = 20$ day spectrum (Figure 15). Moreover, SN 2000cx lacks the Fe II $\lambda 5535$ absorption in the $t = 20$ day spectrum.

The slow change in the ionization stages of Fe is consistent with the prominent “dip” and faint secondary peak evolution for the I -band light curve of SN 2000cx, as discussed in §2.

The evolution of the Si II lines in the spectra of SN 2000cx is also peculiar during this time. Si II $\lambda 6355$ is strong and keeps a P-Cygni profile until $t = 20$ days (Figure 15). This is different from most other SNe Ia, whose Si II $\lambda 6355$ line usually shows progressive contamination by Fe II lines at the blue and the red wings. Figure 15 demonstrates that Fe II lines totally replaced Si II $\lambda 6355$ in SN 1997br, while they seriously contaminated the blue and the red wings of the Si II $\lambda 6355$ line in SN 1994D. While the P-Cygni profile of Si II $\lambda 6355$ in SN 2000cx could be explained by the weakness of the Fe II lines, there is other evidence for strong Si II lines in the spectrum. The Si II $\lambda 5972$ and Na I D blend in SN 2000cx is much stronger than that in SN 1994D and SN 1997br (Figures 14 and 15). The Si II $\lambda 5051$ line is also prominent. In fact, because of the strength of this Si II line, and the weak Fe II $\lambda 5108$ line, the spectral range between 4600 and 5200 \AA forms a broad absorption trough in the $t = 20$ day spectrum of SN 2000cx (Figure 15), in direct contrast to the two emission lines in the spectra of SNe 1994D and 1997br.

3.3. Entering the Nebular Phase

The most important spectral evolution of SN 2000cx during $t = 23$ to 32 days (Figures 10 and 11) is the emergence of the Fe II lines and the weakening of the Si II lines. Fe II $\lambda 4555$ appears at $t = 20$ days and develops into a P-Cygni profile. The Fe II $\lambda 5169$ line also replaces Fe III $\lambda 5129$. The Fe II lines at the blue and the red wings of Si II $\lambda 6355$ appear and strengthen over the time. The Si II lines, on the other hand, become progressively weaker. Si II $\lambda 6355$ almost disappears in the $t = 32$ day spectrum, while the Si II $\lambda 5972$ plus Na I D blend at 5750 \AA becomes progressively weaker, most likely due to the decline of Si II $\lambda 5972$. The weakening of Si II $\lambda 5051$ and the strengthening of Fe II enable the two emission lines to appear between 4600 \AA and 5200 \AA , similar to those of other SNe Ia. By $t = 32$ days (Figure 16), the spectrum of SN 2000cx looks very similar to that of SN 1994D, although there are still subtle differences in the line intensities.

In the $t = 32$ day spectrum of SN 2000cx (Figure 16), there seems to be additional absorption at the blue side of Ca II H & K, which might be caused by Co II $\lambda 3755$, or Ti II $\lambda 3760$, or a high expansion velocity component of Ca II H & K. The identification of Si II $\lambda 3858$ is less plausible, since all the other Si II lines are weak in the spectrum and become weaker, and this feature seems to strengthen from $t = 32$ to 42 days. This line weakens after $t = 42$ days and vanishes at $t \approx 98$ days (Figure 11). The evolution of this feature appears unique to SN 2000cx – we could not find other SNe Ia that have a similar line, either in the literature or in our own spectral database. Understanding the evolution of this line through detailed spectral synthesis may provide clues to the nature of SN 2000cx.

The Ca II IR triplet absorption is stronger in SN 2000cx than in SNe 1994D and 1997br. Inclusion of the absorption marked “?” in Figure 16 as part of the Ca II IR triplet line may strengthen our earlier suggestion that the two blue wiggles in Figure 13 are caused by Ca, although our spectra do not show clearly how those wiggles evolved.

One explanation of the strengthening of the Fe II lines and the weakening of the Si II lines during this period is that the ejecta of SN 2000cx have expanded and become optically thin for the intermediate-mass elements, and the photosphere has receded into the

region with more iron-peak elements. Alternatively, the temperature of the ejecta may have dropped enough to make most iron-peak materials singly ionized. We think both of these causes may contribute to the spectral appearance of SN 2000cx during this period.

After $t = 32$ days the spectral evolution of SN 2000cx is relatively slow, and not very different from that of normal SNe Ia. Apart from the absorption at the blue side of Ca II H & K, the other major change is the development of strong absorption lines in the 7500 – 9000 Å region. These are caused by a combination of O I $\lambda 7773$, the Ca II IR triplet, and O I $\lambda 9264$. Figure 17 shows a comparison of the late-time ($t > 100$ days) spectra of SNe 1991T, 1994D, and 2000cx, with SN 2000cx having the strongest absorption in the red. The development of these absorption lines might cause the fast decline in the *I*-band photometry at $t > 30$ days. Although spectra of SNe Ia at this stage do not have a well-defined continuum, the SN 2000cx spectrum in Figure 17 still seems to be the bluest of the three, consistent with the late-time color evolution of SN 2000cx.

3.4. Expansion Velocities

The expansion velocities (V_{exp}) as inferred from observed minima of absorption lines in the spectra may provide some clue to the nature of SN Ia explosions (Branch, Drucker, & Jeffery 1988). Figure 18 shows the expansion velocities derived from several lines. The Fe III lines of SN 2000cx not only last the longest, but also yield the highest expansion velocities. The V_{exp} derived from the Fe III $\lambda 4404$ line is higher by about 1,000 km s⁻¹ for SN 2000cx than for SN 1991T, while it is higher by about 2,000 km s⁻¹ from the Fe III $\lambda 5129$ line. Fe II $\lambda 4555$ also yields a V_{exp} for SN 2000cx that is about 1,000 km s⁻¹ higher than those for SNe 1991T and 1994D. The V_{exp} derived from the Fe III $\lambda 5129$ line seem to be systematically higher by about 2,000 km s⁻¹ than those from the Fe III $\lambda 4404$ line, which is probably caused by the blending of Fe III $\lambda 5129$ with Si II $\lambda 5051$.

The S II $\lambda 5468$ line does not always have a well-defined profile, so the corresponding V_{exp} measurements for SN 2000cx have a large scatter. Nevertheless, they are systematically higher by about 2,000 to 3,000 km s⁻¹ than those for SNe 1991T (only one point) and

1994D. The values of V_{exp} from S II $\lambda\lambda 5612, 5654$ for SN 2000cx are quite self-consistent and are higher by about $2,000 \text{ km s}^{-1}$ than those of SNe 1991T (only one point) and 1994D.

The V_{exp} measurements from Si II $\lambda 6355$ for SN 2000cx show a unique flat evolution – they remain nearly constant at $12,000 \text{ km s}^{-1}$ from $t = -3$ to 40 days, while all the other SNe Ia in Figure 17 exhibit a gradual decline in V_{exp} . Moreover, the expansion velocities for SN 2000cx are the highest among all the SNe Ia in the comparison sample. These facts perhaps suggest that the Si zone in the expanding ejecta of SN 2000cx was confined to a fairly restricted layer characterized by velocities around $12,000 \text{ km s}^{-1}$.

The higher expansion velocities of SN 2000cx imply more kinetic energy if the mass of its ejecta is similar to that of other SNe Ia. This implication will be used in our discussions of the theoretical models for SN 2000cx.

In summary, the spectral evolution of SN 2000cx is unique. The change of the excitation stage for Fe is unusually slow – the Fe III lines are present in the spectra until $t \approx 15$ days, while the Fe II lines are weak in the spectra until $t \approx 23$ days. The Si II lines are weak in the premaximum spectra, but strengthen over time until $t \approx 7$ days, and stay relatively strong until $t \approx 20$ days. The evolution of the Ca II IR triplet is also peculiar, showing wiggles in the spectra near maximum brightness and strong absorption at late times. SN 2000cx also has high expansion velocities.

4. DISCUSSION

4.1. Absolute Magnitudes

4.1.1. Absolute Magnitudes from Distance Estimates

The host galaxy of SN 2000cx, NGC 524, is the central galaxy in the compact group CfA 13 of Geller & Huchra (1983). The mean heliocentric radial velocity of the eight known group members is 2476 km s^{-1} , with a line-of-sight dispersion $\sigma_V \approx 205 \text{ km s}^{-1}$. The heliocentric velocity of NGC 524 itself (2421 km s^{-1} from NED) is just 55 km s^{-1} smaller,

i.e., within $\sim (1/4)\sigma_V$ of the group mean. In addition, NGC 524 is at (or close to) the projected geometric center of the group, and is almost as luminous as all the other group members combined. In short, NGC 524 is a giant galaxy dominating its surrounding cluster of galaxies.

Based on results from the 1.2 Jy *IRAS* survey (assuming $\beta = 0.5$ in a linear perturbation theory), M. Davis (2001, private communication) concludes that NGC 524 does not participate in the local bulk flow of the Local Group region, but is infalling to the Perseus-Pisces supercluster, and has a predicted outflow of 418 ± 200 km s⁻¹ in the Local Group frame. The corrected recession velocity of NGC 524 in the Local Group frame is 2192 ± 200 km s⁻¹. Thus, we find a distance of 34 ± 3 ($H_0/65$) Mpc and a distance modulus of $\mu = (m - M) = 32.64(\pm 0.20) - 5 \log(H_0/65)$ mag.

Using the apparent peak magnitudes listed in Table 4, together with our estimates of the extinction and distance, we derive the peak absolute magnitudes of SN 2000cx in all filters in Table 6 (under category “from distance estimates”). We adopt H_0 from Parodi et al. (2000; 58.5 km s⁻¹ Mpc⁻¹), but do not include the uncertainty in H_0 in the error analysis. Compared to the absolute magnitudes for a normal SN Ia from Parodi et al. (2000), those of SN 2000cx are overluminous by 0.22, 0.34, and 0.13 mag in M_B , M_V , M_I , respectively.

4.1.2. Absolute Magnitudes from Light-Curve Fits

In earlier discussions we speculated that the peculiar photometric evolution of SN 2000cx might challenge the light-curve fitting techniques for SNe Ia. Here we present more details.

There is a fairly large scatter among the published absolute magnitudes for a normal SN Ia (e.g., Vaughan et al. 1995; Riess, Press, & Kirshner 1996; Saha et al. 1999; Phillips et al. 1999; Parodi et al. 2000), most of which is caused by the different methods used to estimate the reddenings of the SNe Ia. To facilitate discussion, throughout this paper

Table 6. Absolute peak magnitudes of SN 2000cx^a

Method	μ	M_B	M_V	M_R	M_I
From distance estimates					
$v_{CMB} (H_0 = 58.5)$	32.87 ± 0.21	-19.77 ± 0.41	-19.87 ± 0.21	-19.70 ± 0.21	-19.38 ± 0.21
From light-curve fits					
MLCS ^b	32.53 ± 0.35	-19.61 ± 0.21	-19.59 ± 0.21	–	-19.31 ± 0.22
Stretch (–8 to 32d)	–	-19.43 ± 0.20	-19.43 ± 0.17	–	-19.20 ± 0.18
Stretch (–8 to 1d)	–	-19.31 ± 0.12	-19.35 ± 0.10	–	-19.21 ± 0.14
Stretch (1 to 32d)	–	-19.72 ± 0.14	-19.68 ± 0.12	–	-19.35 ± 0.15
$\Delta m_{15}(B)$	–	-19.70 ± 0.14	-19.66 ± 0.12	–	-19.34 ± 0.15
Two-params ^c	–	-19.48 ± 0.14	-19.54 ± 0.10	–	-19.24 ± 0.12

^aSee text for details.

^bThe absolute magnitudes for a normal SN Ia are adopted from Parodi et al. (2000).

^cThe two-parameter luminosity correction method. The luminosity corrections are derived from the parameterization of Drenkhahn & Richtler (1999), and the absolute magnitudes for a normal SN Ia are adopted from Parodi et al. (2000).

we adopt the absolute magnitudes for a normal SN Ia from the weighted mean of eight SNe Ia calibrated through Cepheid distances of their parent galaxies (Parodi et al. 2000): $M_B = -19.55 \pm 0.07$ mag, $M_V = -19.53 \pm 0.06$ mag, and $M_I = -19.25 \pm 0.09$ mag. *The light-curve fitting techniques are only used to derive the luminosity corrections to these absolute magnitudes.* The weighted mean $\Delta m_{15}(B)$ of the eight calibrated SNe Ia is 1.08 ± 0.02 mag. Several light-curve fitting techniques correct the absolute magnitudes of SNe Ia to a “standard SN Ia” with $\Delta m_{15}(B) = 1.10$ mag, and we do not attempt to reconcile the small difference (0.02 mag) in those two $\Delta m_{15}(B)$ values. The R -band absolute magnitude is not well studied in the SNe Ia calibrated with Cepheid variables, and it will not be considered in most of our discussions.

Phillips et al. (1999) used the “Lira-Phillips law” to study the reddening of a sample of 62 SNe Ia, and revised the absolute magnitude vs. $\Delta m_{15}(B)$ relation in a quadratic form. Using the measured $\Delta m_{15}(B)$ of SN 2000cx (0.93 ± 0.04 mag) and equations 20 through 22 in Phillips et al. (1999), we derive the luminosity corrections for SN 2000cx when it is adjusted to a standard decline rate of $\Delta m_{15}(B) = 1.1$ mag: $\Delta M_B^{cor} = -0.15 \pm 0.08$ mag, $\Delta M_V^{cor} = -0.13 \pm 0.08$ mag, and $\Delta M_I^{cor} = -0.09 \pm 0.07$ mag. These numbers indicate that SN 2000cx is slightly overluminous compared with a normal SN Ia with $\Delta m_{15}(B) = 1.1$ mag. Using the absolute magnitudes of a normal SN Ia from Parodi et al. (2000), we derive the absolute magnitudes of SN 2000cx to be $M_B = -19.70 \pm 0.14$ mag, $M_V = -19.66 \pm 0.12$ mag, and $M_I = -19.34 \pm 0.15$ mag.

We have done a MLCS fit to SN 2000cx and the results are shown in the left panel of Figure 19. This is the worst MLCS fit we have ever seen for a SN Ia. While the V and R fits may be marginal, the B and I fits are poor. The model B -band light curve peaks about two days earlier than the observed one, and the slow decline in the observations is not reproduced. In the I band the deep decline after the first peak is not reproduced by the model. It is clear that the photometric evolution of SN 2000cx does not conform to the family of SNe Ia constructed in MLCS.

The MLCS fit reports a distance modulus to SN 2000cx of $\mu = 32.53 \pm 0.35$ mag, and a “luminosity correction” $\Delta = -0.06 \pm 0.20$ mag. This distance modulus is slightly smaller

than, but within the uncertainties of, the ones estimated from the recession velocity of NGC 524. The derived absolute magnitudes of SN 2000cx are $M_B = -19.61 \pm 0.21$ mag, $M_V = -19.59 \pm 0.21$ mag, and $M_I = -19.31 \pm 0.22$ mag if the absolute magnitudes of a normal SN Ia from Parodi et al. (2000) are used. Considering the poor MLCS fit, however, these values may not be representative of SN 2000cx.

The right panel of Figure 19 shows three fits to the peak of the B -band light curve of SN 2000cx ($t = -8$ to 32 days) using the “stretch method” (Perlmutter et al. 1997). The normalized flux for the B -band template is adopted from the “Parab-18” model of Goldhaber et al. (2001). The solid, dash-dotted, and dashed lines are the fits for all the data points ($t = -8$ to 32 days), the premaximum data points ($t = -8$ to 1 day), and the postmaximum data points ($t = 1$ to 32 days), respectively. The stretch factors (s) derived are 0.89 ± 0.06 (solid line), 0.76 ± 0.01 (dash-dotted line), and 1.09 ± 0.02 (dashed line), and the corresponding $\Delta m_{15}(B)$ values are 1.27 ± 0.18 mag, 1.64 ± 0.02 mag, and 0.91 ± 0.03 mag, respectively (measured from the fitted curve). We note that the solid line (the fit to all the data points from $t = -8$ to 32 days) does not reproduce the observations well: it rises a little bit too slowly, and declines too fast between $t = 10$ and 30 days. The dash-dotted ($s = 0.76 \pm 0.01$) and the dashed ($s = 1.09 \pm 0.02$) lines fit the observations very well, but yield very different stretch factors. SN 2000cx is clearly a counterexample to the results of Goldhaber et al. (2001), who claim that a single stretch factor applies equally well to the rising and declining parts of the light curve.

Using the $\Delta m_{15}(B)$ value measured from the fitted curves and the prescription of Phillips et al. (1999), we derive the absolute magnitudes for SN 2000cx from the stretch method and present them in Table 6, together with results from the absolute magnitude vs. $\Delta m_{15}(B)$ relation and MLCS (under category “from light-curve fits”). The stretch method yields quite different absolute magnitudes for SN 2000cx when different parts of the light curve are used in the fit. For example, the fit to the premaximum observations indicates that SN 2000cx is subluminous, while the fit to the postmaximum observations suggests an overluminous event.

One notices that the mismatch between the fit (from both MLCS and the stretch

method) and the data is revealed by the excellent temporal coverage of the SN 2000cx observations. If the observations were more sparse, a better fit could be achieved and the mismatch would not be noticed. Since most of the observed SNe Ia generally do not have such dense temporal coverage, it is important to understand the nature of objects like SN 2000cx and to investigate how frequent they are, so as to assess the contamination of the observed SN Ia sample (at both low and high redshifts) by these objects (although there are about a dozen normal SNe Ia with sampling like SN 2000cx that are fit well by MLCS).

A two-parameter luminosity correction method was developed recently (e.g., Tripp & Branch 1999; Drenkhahn & Richtler 1999). This method corrects the absolute magnitudes of a SN Ia according to both its $\Delta m_{15}(B)$ and its color ($B_{max} - V_{max}$), where B_{max} and V_{max} are the maximum apparent B and V magnitudes of the SN *corrected only for the Galactic reddening*. Using the parameterization of Drenkhahn & Richtler (1999) for the luminosity corrections [to a standard SN Ia with $\Delta m_{15}(B) = 1.10$ mag] and our adopted absolute magnitudes of a normal SN Ia from Parodi et al. (2000), we derive the following absolute magnitudes for SN 2000cx: $M_B = -19.48 \pm 0.14$ mag, $M_V = -19.54 \pm 0.10$ mag, and $M_I = -19.24 \pm 0.12$ mag. These values are listed in Table 6 as entry “two-params.”

There is one caveat in the two-parameter luminosity correction method: it does not differentiate between the host-galaxy reddening and the intrinsic color of SNe Ia. In other words, a red ($B_{max} - V_{max}$) color for a SN Ia may be caused by the host-galaxy reddening to the SN, or the SN may be intrinsically red. Since we cannot expect the correction coefficients to be the same for the host-galaxy reddening (which should have coefficients based on the reddening law of dust) and the intrinsic color (which should have coefficients determined from the physics of SNe Ia), it may be difficult or impossible to apply the method to an individual SN Ia. A good indication of the effect of neglecting the difference between the host-galaxy reddening and the intrinsic color of SNe Ia is provided by the derived coefficients for ($B_{max} - V_{max}$): only 2.1 to 2.5 in the corrections for M_B , much smaller than the coefficient used in the canonical Galactic reddening law (4.1). A better approach is to differentiate between the host-galaxy reddening and the intrinsic color of SNe Ia, and use different coefficients for the corrections. However, there is no excellent, general

method for estimating the host-galaxy reddening to SNe Ia. For example, the “Lira-Phillips law” (Phillips et al. 1999), though easy to implement, may suffer from uncertainties larger than initially estimated, as discussed earlier in this paper.

In summary, the light-curve fitting techniques currently available (MLCS and the stretch method) fail to reproduce the photometric behavior of SN 2000cx. The absolute magnitude vs. $\Delta m_{15}(B)$ relation and the two-parameter luminosity correction method use only information derived from light curves of SNe Ia and do not attempt to fit them, so it is difficult to assess the accuracy of the values derived from these two methods. In the next section, we will estimate the absolute magnitudes of SN 2000cx from theoretical model considerations and compare them to those measured here.

Surprisingly, Table 6 indicates that despite all the difficulties in fitting the light curves of SN 2000cx, different techniques yield results with reasonably small scatter. The weighted mean absolute magnitudes of SN 2000cx are $M_B = -19.53 \pm 0.15$ mag, $M_V = -19.53 \pm 0.13$ mag, and $M_I = -19.27 \pm 0.09$ mag, which are very similar to the values for normal SNe Ia in Parodi et al. (2000).

4.2. Theoretical Models for SN 2000cx

SNe Ia are widely believed to be thermonuclear explosions of mass-accreting carbon-oxygen (C-O) white dwarfs (WDs). The conversion of carbon and oxygen to iron-peak and intermediate-mass elements releases a large amount of energy initially, thereby disrupting the star, and subsequently the radioactive decay of ^{56}Ni to ^{56}Fe powers the supernova through γ -ray photons and positrons. Despite more than half a century of observations and theoretical studies, however, an understanding of the detailed physics leading to SN Ia explosions remains elusive. SNe Ia explosion models are frustrated by two main issues, the uncertainties about thermonuclear flame physics and the progenitor evolution.

Currently, three explosion scenarios dominate the theoretical models of SNe Ia. (1) The first (referred to as the “single-degenerate model”) consists of a C-O WD near the

Chandrasekhar mass accreting hydrogen or helium from a non-degenerate companion until it reaches a mass at which the core carbon ignites. If the subsequent burning front accelerates to become a detonation in the outer layers of the WD, a “delayed detonation” results. If the burning front remains subsonic, the result is a “deflagration.” These single-degenerate models account for observed inhomogeneities through variations in the propagation of the burning front due to density and/or compositional differences in the C-O WD progenitor. (2) The second scenario (referred to as the “double-degenerate model”) merges two C-O WDs, with the more massive WD accreting the companion. The range of masses of these explosions has been suggested to vary from 1.2 to 1.8 M_{\odot} , explaining the observed inhomogeneities of SNe Ia. (3) The third scenario (referred to as the “sub-Chandrasekhar model”) consists of a lower-mass C-O WD accreting a helium shell, which becomes thick enough to produce a helium shell detonation. Observed differences among SNe Ia are explained in this model by the different nucleosynthesis that results when the progenitor mass varies from 0.65 to 1.1 M_{\odot} .

The pros and cons of these scenarios are not the subject of this paper; for reviews see Branch et al. (1995) and Livio (2000). It is worth noting, however, that Branch (2001) concludes that recent developments favor the single-degenerate model for SNe Ia. Years of tuning the single-degenerate models to achieve a match between observed and computed spectra and light curves have also resulted in a list of distinct properties which the “successful” SN Ia explosion model must possess. Successful ones include deflagration model W7 (Nomoto, Thielemann, & Yokoi 1984) and delayed-detonation model DD4 (Woosley & Weaver 1994; Pinto & Eastman 2001, hereafter PE2001).

PE2001 used the DD4 model and its variants to study the correlation between luminosity and light-curve width among SNe Ia [similar studies have been conducted by Höflich, Khokhlov, & Wheeler (1995) and Höflich & Khokhlov (1996)]. Their DD4 models yield ^{56}Ni ranging from 0.27 to 0.90 M_{\odot} , and peak absolute V from -18.90 to -19.78 mag. They are able to reproduce the observed absolute magnitude vs. $\Delta m_{15}(B)$ relation [although in their Figure 2 they used $\Delta m_{15}(B)$ measured from the modeled V -band light curve, i.e., it is actually $\Delta m_{15}(V)$] and found it to be a natural consequence of the radiation

transport in SNe Ia, with the ^{56}Ni production and the γ -ray escape fraction during the explosion being the dominant factors. For example, more ^{56}Ni leads to more heating, higher temperatures, less efficient cooling, and hence broader and brighter light curves, while larger γ -ray escape fractions (e.g., models with higher overall velocities and/or with ^{56}Ni distributions extending to higher velocities) lead to narrower light curves. Since larger ^{56}Ni production and higher velocities tend to produce opposite effects on light curves of SNe Ia, the solution is not unique for a particular SN unless additional constraints are obtained from observations.

We are particularly interested in PE2001’s model DD3 (initially studied by Woosley & Weaver 1991), a variant of model DD4/90 which has a ^{56}Ni production of $0.90 M_{\odot}$, a peak V absolute magnitude of -19.78 , and a $\Delta m_{15}(V)$ of 0.87 mag. Compared to model DD4/90, model DD3 has greater production of ^{56}Ni ($0.96 M_{\odot}$), a larger total amount of burning, and higher velocities for the ejecta; it burns 10% more mass to the Si-group or above and has 10% greater kinetic energy than model DD4/90. In spite of its high ^{56}Ni mass, the light curve from model DD3 is considerably narrower than that of model DD4/90. The higher kinetic energy in the explosion of model DD3 results in a lower column depth, allowing γ -rays to escape more easily. At around maximum optical brightness, $\sim 6\%$ of the decay energy in model DD4/90 escapes directly as γ -rays, increasing to 35% by $t \approx 20$ days. In model DD3, the escape fraction is more than double that of model DD4/90 around maximum, at $\sim 14\%$, rising to 46% by $t \approx 20$ days. A shortened time to γ -ray transparency for model DD3 leads to a faster rising phase, a narrower peak, and a greater decline rate at late times. The increased γ -ray escape is, however, more than compensated by the faster rise and narrower peak, and the luminosity at peak ($M_V = -19.90$ mag) is even brighter than the difference one might predict based on consideration of the difference in total ^{56}Ni mass. Model DD3 has the same postmaximum decline rate as model DD4/90 [$\Delta m_{15}(V) = 0.87$ mag].

We propose that the comparison of SN 2000cx to SN 1991T is analogous to that of model DD3 to model DD4/90. SN 2000cx and SN 1991T have very similar postmaximum decline rates $\Delta m_{15}(B)$. Since SN 2000cx has much higher expansion velocities for both

the intermediate-mass and iron-peak elements than SN 1991T does (Figure 18), it has a smaller column density and a larger γ -ray escape fraction. The similar $\Delta m_{15}(B)$ for the two SNe thus indicates that SN 2000cx synthesized more ^{56}Ni during the explosion than did SN 1991T. Mazzali, Danziger, & Turatto (1995) estimated that $\sim 1M_{\odot}$ of ^{56}Ni was produced in the explosion of SN 1991T, so SN 2000cx may have synthesized more than $1M_{\odot}$ of ^{56}Ni , the largest ever found for a SN Ia. In spite of its higher ^{56}Ni mass, the light curve is considerably narrower than that of SN 1991T because the higher kinetic energy in SN 2000cx results in a lower column depth, allowing γ -rays to escape more easily. The faster rising phase, and the greater late-time decline rate in the *BVRI* passbands (§2), are all indications of a larger γ -ray escape fraction.

Spectroscopically, the strong resemblance of the premaximum spectra of SN 2000cx to those of SN 1991T provides additional evidence that the two SNe are closely related. The prominence of Fe III lines and the lack of strong Si II, S II, and Ca II lines at these early times is explained mainly by a composition effect (Filippenko et al. 1992b; Ruiz-Lapuente et al. 1992; Jeffery et al. 1992), a temperature effect (Nugent et al. 1995), or both (Mazzali, Danziger, & Turatto 1995). The spectra of SN 2000cx indicate that both the iron-peak and the intermediate-mass elements are moving at high expansion velocities in the outer layers of the ejecta (Figure 18), suggesting that both the composition and the temperature significantly affect the formation of the spectral lines at this time. In other words, the strong Fe III lines may be caused by the composition abnormality of iron-peak elements in the outer layers of the ejecta, but the lack of strong lines of the intermediate-mass elements is caused by the high radiation temperature, not the physical absence of such elements.

As discussed in §3, although SNe 2000cx and 1991T have similar premaximum spectra, their overall spectral evolution is quite different. This is almost certainly caused by differences in the ^{56}Ni mass and the expansion velocities of the ejecta. SN 2000cx has a higher ^{56}Ni mass and hotter ejecta, but the faster expansion velocities yield a larger γ -ray escape fraction so the continua of the observed spectra are not particularly blue (in fact, the color at the earliest epochs is redder than that of SN 1991T; §3). The temperature of the photosphere of SN 2000cx must have been dropping from $t = -3$ days to a week after

maximum brightness, as the features of the intermediate-mass elements (in particular Si and S) grow stronger.

The peculiar photometric and spectroscopic evolution of SN 2000cx during $t = 6$ to 15 days [i.e., the transition phase in the B -band light curve, the plateau phase in the $(B - V)_0$ color, the bluest part of the $(V - R)_0$ and $(V - I)_0$ color, the prominent Fe III and Si II lines, and the blue continuum], might be due to changes in the ratio of the γ -ray escape fraction of SN 2000cx relative to SN 1991T. As demonstrated by models DD3 and DD4/90, the ratio of the γ -ray escape fraction of model DD3 to that of model DD4/90 is $\sim 230\%$ around maximum, and it drops to only $\sim 130\%$ at $t \approx 20$ days. For SN 2000cx, the drop of this ratio means its continuum formation does not differ much from that of other SNe Ia, and its high intrinsic radiation temperature (which is supported by the strength of the Fe III lines) yields a much bluer continuum. This is also the reason why the $(V - R)_0$ and $(V - I)_0$ colors are so blue; they are sensitive to the continuum shape. The $(B - V)_0$ color stays nearly constant during this period because, as discussed in §3, the change in the continuum shape is compensated by variations in the spectral features. The decrease of the ratio of the γ -ray escape fraction may also be the reason for the transition phase in the B -band light curve.

The late-time spectral and photometric evolution of SN 2000cx can also be understood in terms of a higher radiation temperature and a larger γ -ray escape fraction. The higher radiation temperature explains the unusual blue color evolution at late times, while the larger γ -ray escape fraction is responsible for the steeper decline rate in the late-time $BVRI$ light curves.

We should note that even though the delayed detonation model DD3 (a single-degenerate model) seems to account for the observations of SN 2000cx quite well, the essence of the model (high ^{56}Ni mass and high expansion velocity of the ejecta) could be produced in other scenarios as well. For example, Filippenko et al. (1992b) suggested a double-detonation model for SN 1991T, in which a mildly sub-Chandrasekhar mass WD is nearly completely incinerated by detonation waves propagating inward and outward from the base of an accumulated helium layer. This model is capable of producing a large

amount of ^{56}Ni because of the complete burning to iron-peak elements by detonation. The outward detonation also produces material moving at high expansion velocities. However, the presence of intermediate-mass elements at high velocities, and the persistent strong Si II lines during $t = 7$ to 20 days, seem to contradict nucleosynthesis from complete detonations. Fisher et al. (1999) used a super-Chandrasekhar explosion from the merger of two WDs as the origin of SN 1991T. The expected strong explosion from a super-Chandrasekhar WD could produce large amounts of ^{56}Ni , and a high-velocity iron-peak core surrounded by a small mass of intermediate-mass elements; this encounters a surrounding low-density mass of carbon and oxygen of the companion WD which decelerates the intermediate-mass elements and forces them into a narrow velocity interval. Our spectra of SN 2000cx indicate that the intermediate-mass elements are indeed confined to a fairly restricted layer characterized by velocities around $12,000 \text{ km s}^{-1}$. Although the necessity of a super-Chandrasekhar explosion for SN 1991T is questionable after the Cepheid distance to its host galaxy NGC 4527 was measured (Saha et al. 2001) and SN 1991T was found to be only mildly overluminous compared to normal SNe Ia, the super-Chandrasekhar explosion may be a viable model for SN 2000cx. There are, however, few studies of this model in the literature, so a detailed comparison with our observations cannot be made.

We also emphasize that since there are still relatively large uncertainties in the theoretical models for SNe Ia (e.g., details about thermonuclear flame physics and the progenitor evolution), our comparison of SN 2000cx and SN 1991T, and the analog of the comparison of model DD3 and DD4/90, are only qualitative. A comprehensive quantitative study should involve detailed modeling of spectra and multicolor light curves of model DD3, and comparison with the observations of SN 2000cx. This is beyond the scope of the current paper. It is worth noting, however, that the comparison between model DD3 and DD4/90 is done in the V band in PE2001, while our comparison concentrated mostly on the B -band observations of SN 2000cx. It is unclear whether the correlations in the V band reported by PE2001 apply to the B band as well. Moreover, SN 2000cx is very distinct from SN 1991T in the V , R , and I passbands (Figures 4, 5, and 6), so they may be quite different objects.

4.3. Implications of the SN 2000cx Observations

If we accept the theoretical connection between SN 2000cx and SN 1991T discussed above, SN 2000cx should have absolute magnitudes brighter than those of SN 1991T by about 0.1 mag as indicated by the difference in models DD3 and DD4/90. Adopting the absolute magnitudes of SN 1991T from Saha et al. (2001) [they assumed a reddening of $E(B - V) = 0.2 \pm 0.1$ mag to SN 1991T], the absolute magnitudes for SN 2000cx are $M_B = -19.96 \pm 0.36$, $M_V = -19.95 \pm 0.29$ mag, and $M_I = -19.55 \pm 0.21$ mag.

The absolute magnitudes derived from distance estimates and the light-curve fitting techniques (Table 6) are systematically fainter than the theoretical expectations. This indicates that NGC 524 may be more distant than estimated from its recession velocity. On the other hand, given the bad fits discussed earlier, the difference between the estimates from the theoretical models and those from the light-curve fitting techniques is not surprising, and the estimates are still consistent within their uncertainties. The closest match to the estimates from the theoretical models are those derived from the recession-velocity distance with $H_0 = 58.5 \text{ km s}^{-1} \text{ Mpc}^{-1}$, from the stretch method fit to the postmaximum data points, and from the luminosity vs. $\Delta m_{15}(B)$ relation.

If the expansion velocity of a SN Ia affects its light-curve shape, as suggested by PE2001, the current luminosity vs. light-curve width relation should be revised by taking into account the expansion velocities of SNe Ia. Since higher V_{exp} reduces the light-curve width and increases the $\Delta m_{15}(B)$ value¹⁰, given the same $\Delta m_{15}(B)$ value the corrected luminosity should be higher for a SN Ia with higher V_{exp} . There is a trend that SNe Ia in late-type galaxies have higher V_{exp} (Filippenko 1989; Branch & van den Bergh 1993) and higher luminosity (Hamuy et al. 2000) than those in early-type galaxies, so the V_{exp} -corrected luminosity vs. light-curve width relation will have a steeper slope than currently assumed.

¹⁰Although the Δm_{15} value of model DD3 is the same as that of model DD4/90, it is relatively too large for the higher luminosity and larger ^{56}Ni mass of model DD3.

We emphasize again that the above conclusion is based on the result by PE2001 that the expansion velocity affects the light-curve formation. More theoretical studies need to be conducted to verify this result, and to provide a quantitative guide on how to correct the current luminosity vs. light-curve width relation.

One interesting question is how frequent SN 2000cx-like objects are. SN 2000cx is clearly a peculiar SN Ia, perhaps closely related to SN 1991T-like objects. Li et al. (2001) studied a well-understood sample of SNe Ia and concluded that the rate of peculiar SNe Ia such as SN 1991T and SN 1991bg (Filippenko et al. 1992a) may constitute a significant fraction of the observed SNe Ia ($\sim 20\%$ are SN 1991T-like and $\sim 16\%$ are SN 1991bg-like). We failed to find a SN Ia similar to SN 2000cx, however, both in the literature and in our photometric database, so objects like SN 2000cx may be very rare and originate only under extreme conditions. Such mavericks, however, may reveal trends that are otherwise buried in observational uncertainties.

Another interesting question is whether the peculiarity of SN 2000cx is related to the nature of its environment. SN 2000cx is located very far away from the nucleus of its host galaxy, where the metallicity is likely to be low given the abundance gradients observed in galaxies (Henry & Worthey 1999). Hamuy et al. (2000) suggested that metal-poorer environments produce the most luminous SNe Ia, which is supported by SN 2000cx if it is indeed more luminous than SN 1991T. On the other hand, Ivanov, Hamuy, & Pinto (2000) studied the radial distribution of SNe Ia and showed that there is no indication of systematic changes of the luminosity of SNe Ia with radial distance, suggesting that the metallicity effects on SNe Ia are likely to be small.

5. CONCLUSIONS

(1) SN 2000cx is a very peculiar object – indeed, unique among all known SNe Ia. The light curves cannot be fit well by any of the fitting techniques currently available (e.g., MLCS and the stretch method). There is an apparent asymmetry in the rising and declining parts of the B -band light curve, while there is a unique “shoulder”-like evolution

in the V -band light curve. The R -band and I -band light curves have relatively weak second maxima. In all $BVRI$ passbands the late-time decline rates are relatively large compared to other SNe Ia.

(2) SN 2000cx has the reddest $(B - V)_0$ color before $t \approx 7$ days among several SNe Ia, and it subsequently has a peculiar plateau phase where $(B - V)_0$ remains at 0.3 mag until $t = 15$ days. The late-time $(B - V)_0$ evolution of SN 2000cx is found to be rather blue, and is inconsistent with the fit proposed by Lira (1995) and Phillips et al. (1999). SN 2000cx also has very blue $(V - R)_0$ and $(V - I)_0$ colors compared to other SNe Ia.

(3) Our earliest spectrum of SN 2000cx ($t = -3$ days) reveals remarkable resemblance to those of SN 1991T-like objects, with prominent Fe III lines and weak Si II lines. As in the case of SN 1991T, Si II lines strengthened around the time of maximum brightness. However, the subsequent spectral evolution of SN 2000cx is quite different from that of SN 1991T. The Fe III and Si II lines remain strong, and the Fe II lines remain weak, in the spectra of SN 2000cx until $t \approx 20$ days, indicating that the excitation stages of iron-peak elements change relatively slowly in SN 2000cx compared to other SNe Ia, and suggesting that the photosphere of SN 2000cx stays hot for a long time. Both iron-peak and intermediate-mass elements are found to be moving at very high velocities in SN 2000cx. The V_{exp} measured from the Si II $\lambda 6355$ line shows a peculiar (nearly constant) evolution.

(4) We find that the delayed detonation model DD3 (Woosley & Weaver 1991) investigated by Pinto & Eastman (2000b) accounts for the observations of SN 2000cx rather well. This model suggests that SN 2000cx is similar to SN 1991T, but with a larger ^{56}Ni production and a higher kinetic energy (i.e., greater expansion velocity for the ejecta). We emphasize that because of uncertainties in the current theoretical models for SNe Ia, various views should be considered. For example, the big difference between SN 2000cx and SN 1991T in their V , R , and I light curves may suggest that they are two very different objects.

We thank the staffs of the Lick Observatory and Wise Observatory for their assistance, and we acknowledge useful conversations with K. Krisciunas and M. Davis. The work of A.V.F.'s group at U. C. Berkeley is supported by the National Science Foundation

grant AST-9987438, as well as by the Sylvia and Jim Katzman Foundation. KAIT was made possible by generous donations from Sun Microsystems, Inc., the Hewlett-Packard Company, AutoScope Corporation, Lick Observatory, the National Science Foundation, the University of California, and the Katzman Foundation. A.V.F. is grateful to the Guggenheim Foundation for a Fellowship. Astronomy at the Wise Observatory is supported by grants from the Israel Science Foundation. The Wise Observatory queue-observing program is made possible by the devoted help of the Wise Observatory staff.

REFERENCES

- Aldering, G., Knop, R., & Nugent, P. 2000, *AJ*, 119, 2110
- Bessell, M. S. 1990, *PASP*, 102, 1181
- Bessell, M. S. 1999, *PASP*, 111, 1426
- Branch, D. 2001, in *Young Supernova Remnants*, eds. S. S. Holt & U. Hwang (New York: AIP)
- Branch, D., et al. 1983, *ApJ*, 270, 123
- Branch, D., Drucker, W., & Jeffery, D. J. 1988, *ApJ*, 330, L117
- Branch, D., & van den Bergh, S. 1993, *AJ*, 105, 2231
- Branch, D., et al. 1995, *PASP*, 107, 1019
- Chornock, R., et al. 2000, *IAU Circ.* 7463
- Coil, A. L., et al. 2000, *ApJ*, 544, L111
- Cousins, A. W. J. 1981, *South African Astron. Obs. Circ.*, 6, 4
- Drenkhahn, G., & Richtler, T. 1999, *A&A*, 349, 877
- Falco, E., et al. 1999, *ApJ*, 523, 617
- Filippenko, A. V. 1982, *PASP*, 94, 715
- Filippenko, A. V. 1989, *PASP*, 101, 588
- Filippenko, A. V. 1997, *ARA&A*, 35, 309
- Filippenko, A. V., Li, W. D., Treffers, R. R., & Modjaz, M. 2001, in *Small Robotic Telescopes*, ed. W. Chen (San Francisco: Astron. Soc. Pacific, Conf. Ser. Vol. 246), in press

- Filippenko, A. V., et al. 1992a, AJ, 104, 1543
- Filippenko, A. V., et al. 1992b, ApJ, 394, L15
- Fisher, A., et al. 1999, MNRAS, 304, 67
- Geller, M. J., & Huchra, J. P. 1983, ApJS, 52, 61
- Goldhaber, G., et al. 2001, ApJ, in press (astro-ph/0104382)
- Hatano, K., et al. 1999, ApJ, 525, 881
- Hamuy, M., et al. 1996a, AJ, 112, 2391
- Hamuy, M., et al. 1996b, AJ, 112, 2408
- Hamuy, M., et al. 2000, AJ, 120, 1479
- Henry, R. B. C., & Worthey, G. 1999, PASP, 111, 919
- Höflich, P. 1991, A&A, 246, 481
- Höflich, P., Khokhlov, A. M., & Wheeler, J. C., 1995, ApJ, 444, 831
- Höflich, P., & Khokhlov, A. M., 1996, ApJ, 457, 500
- Horne, K. 1986, PASP, 98, 609
- Howell, D. A., Wang, L. F., & Wheeler, J. C., 2000, ApJ, 530, 166
- Ivanov, V. D., Hamuy, M., & Pinto, P. A. 2000, ApJ, 542, 588
- Jeffery, D. J., et al. 1992, ApJ, 397, 304
- Jha, S., et al. 1999, ApJS, 125, 73
- Johnson, H. L., et al. 1966, Commun. Lunar Planet. Lab., 4, 99
- Kirshner, R. P., et al. 1993, ApJ, 415, 589

- Landolt, A. U. 1992, *AJ*, 104, 340
- Leibundgut, B., et al. 1993, *AJ*, 105, 301
- Leonard, D. C. 2001, PhD thesis, Univ. of California, Berkeley
- Leonard, D. C., et al. 2001, *IAU Circ.* 7471
- Li, W. D., et al. 2000, in *Cosmic Explosions*, eds. S. S. Holt and W. W. Zhang (New York: American Institute of Physics), p. 103
- Li, W. D., et al. 1999, *AJ*, 117, 2709
- Li, W. D., et al. 2001, *ApJ*, 546, 734
- Lira, P. 1995, Masters thesis, Univ. Chile
- Lira, P., et al. 1998, *AJ*, 115, 234
- Livio, M. 2000, in *Type Ia Supernovae and Cosmology*, eds. J. C. Niemeyer & J. W. Truran (Cambridge: Cambridge Univ. Press), p. 33
- Matheson, T. 2000, PhD thesis, Univ. of California, Berkeley
- Mazzali, P. A., Danziger, I. J., & Turatto, M. 1995, *A&A*, 297, 509
- Miller, J. S., & Stone, R. P. S. 1993, *Lick Obs. Tech. Rep.* 66 (Santa Cruz: Lick Obs.)
- Milne, P. A., The, L.-S., & Leising, M. D. 2001, *astro-ph/0104185*
- Modjaz, M., et al. 2000, *PASP*, 113, 308
- Nomoto, K., Thielemann, F. K., & Yokoi, K. 1984, *ApJ*, 286, 644
- Nugent, P., et al. 1995, *ApJ*, 455, L147
- Parodi, B. R., Saha, A., Sandage, A., & Tammann, G. A. 2000, *ApJ*, 540, 634
- Patat, F., et al. 1996, *MNRAS*, 278, 111

- Perlmutter, S., et al. 1997, ApJ, 483, 565
- Perlmutter, S., et al. 1999, ApJ, 517, 565
- Phillips, M. M. 1993, ApJ, 413, L105
- Phillips, M. M., et al. 1987, PASP, 99, 592
- Phillips, M. M., et al. 1992, AJ, 103, 1632
- Phillips, M. M., et al. 1999, AJ, 118, 1766
- Pinto, P. A., & Eastman, R. G. 2000, ApJ, 530, 757
- Pinto, P. A., & Eastman, R. G. 2001, astro-ph/0006171 (PE2001)
- Richmond, M. W., et al. 1995, AJ, 109, 2121
- Riess, A. G., Press, W. H., & Kirshner, R. P. 1996, ApJ, 473, 88
- Riess, A. G., et al. 1998a, AJ, 116, 1009
- Riess, A. G., et al. 1998b, ApJ, 504, 935
- Riess, A. G., et al. 1999, AJ, 118, 2668
- Riess, A. G., et al. 2000, ApJ, 536, 62
- Riess, A. G., et al. 2001, ApJ, in press (astro-ph/0104455)
- Ruiz-Lapuente, P., et al. 1992, ApJ, 387, L33
- Saha, A., et al. 1999, ApJ, 522, 802
- Saha, A., et al. 2001, ApJ, 551, 973
- Savage, B. D., & Mathis, J. S. 1979, ARA&A, 17, 73
- Schlegel, D. J., Finkbeiner, D. P., & Davis, M. 1998, ApJ, 500, 525

Stetson, P. B. 1987, *PASP*, 99, 191

Suntzeff, N. B. 2000, in *Cosmic Explosions*, eds. S. S. Holt and W. W. Zhang (New York: American Institute of Physics), p. 65

Treffers, R. R., et al. 1997, *IAU Circ.* 6627

Tripp, R., & Branch, D. 1999, *ApJ*, 525, 209

Turatto, M., et al. 1996, *MNRAS*, 283, 1

Vaughan, T. E., Branch, D., Miller, D. L., & Perlmutter S. 1995, *ApJ*, 439, 558

Wells, L. A., et al. 1994, *AJ*, 108, 2233

Woosley, S. E., & Weaver, T. A. 1994, in *Supernovae, Session LIV, Les Houches*, eds. S. Bludman, R. Mochkovitch, & J. Zinn-Justin (Elsevier Science Publishers), p. 63

Yu, C., Modjaz, M., & Li, W. D. 2000, *IAU Circ.* 7458

Fig. 1.— V -band KAIT image of the field of SN 2000cx in NGC 524, taken on 2000 July 25. The field of view is $6'.7 \times 6'.7$. The four local standard stars are marked (1 – 4).

Fig. 2.— The B , V , R , and I light curves of SN 2000cx. The open circles are the KAIT measurements and the solid circles are the WO data. For most of the points the uncertainties are smaller than the plotted symbols.

Fig. 3.— The B -band light curve of SN 2000cx, together with those of SN 1991T (Lira et al. 1998), SN 1991bg (Leibundgut et al. 1993), SN 1992bc (Hamuy et al. 1996b), SN 1992al (Hamuy et al. 1996b), and SN 1994D (Richmond et al. 1995). All light curves are shifted in time and peak magnitude to match that of SN 2000cx. The inset shows the comparison near maximum.

Fig. 4.— Same as Figure 3 but for the V light curve.

Fig. 5.— Same as Figure 3 but for the R light curve. The R light curve of SN 1991bg comes from Filippenko et al. (1992a).

Fig. 6.— Same as Figure 3 but for the I light curve. The I light curve of SN 1991bg comes from Filippenko et al. (1992a).

Fig. 7.— The $(B - V)_0$ color curve of SN 2000cx, together with those of SN 1991T [dereddened by $E(B - V) = 0.13$ mag], SN 1992bc [dereddened by $E(B - V) = 0.02$ mag], SN 1992al [dereddened by $E(B - V) = 0.04$ mag], and SN 1994D [dereddened by $E(B - V) = 0.04$ mag]. The wide line labeled “L-P law” is the fit by Lira (1995) and Phillips et al. (1999).

Fig. 8.— Same as in Figure 7 but for the $(V - R)_0$ color curve.

Fig. 9.— Same as in Figure 7 but for the $(V - I)_0$ color curve.

Fig. 10.— Montage of spectra of SN 2000cx obtained at $t < 30$ days. The phases marked are relative to the date of B maximum (those denoted with a “p” were obtained in spectropolarimetric mode). To improve clarity, the spectra have been shifted vertically by arbitrary amounts. The spectra have been corrected for reddening [$E(B - V) = 0.08$ mag, see text for details] and redshift (2421 km s^{-1}).

Fig. 11.— Same as in Figure 10 but for spectra obtained at $t > 30$ days. The region redward of 7500 \AA has been boxcar smoothed (smoothing box = 5 pixels) for the spectra at days 98, 126, and 148.

Fig. 12.— The spectrum of SN 2000cx at $t = -3$ days, shown with comparable-phase spectra of SN 1994D and SN 1997br. All the spectra illustrated here and in subsequent figures have been dereddened and deredshifted. See text for sources of line identifications.

Fig. 13.— Same as in Figure 12 but for spectra near maximum brightness.

Fig. 14.— Same as in Figure 12 but for spectra around $t = 14$ days. The features marked with a “ \oplus ” in the spectrum of SN 1997br are caused by telluric absorption bands. The four dotted vertical lines are (from left to right) the expected positions of the Fe III $\lambda 4404$, Fe II $\lambda 4555$, Fe III $\lambda 5129$, and Fe II $\lambda 5169$ absorptions. Note the strong Fe III and weak Fe II lines in the spectrum of SN 2000cx.

Fig. 15.— Same as in Figure 12 but for spectra around $t = 20$ days. The two dotted vertical lines are the expected positions of the Fe II $\lambda 4555$ and Fe II $\lambda 5169$ absorptions. Weak Fe II lines begin to develop in the spectrum of SN 2000cx.

Fig. 16.— Same as in Figure 12 but for spectra around $t = 30$ days. The features marked with a “ \oplus ” in the spectrum of SN 1997br are caused by telluric absorption bands. The two dotted vertical lines are the expected positions of the Fe II $\lambda 4555$ and Fe II $\lambda 5169$ absorptions. The Fe II lines are apparent in the spectrum of SN 2000cx.

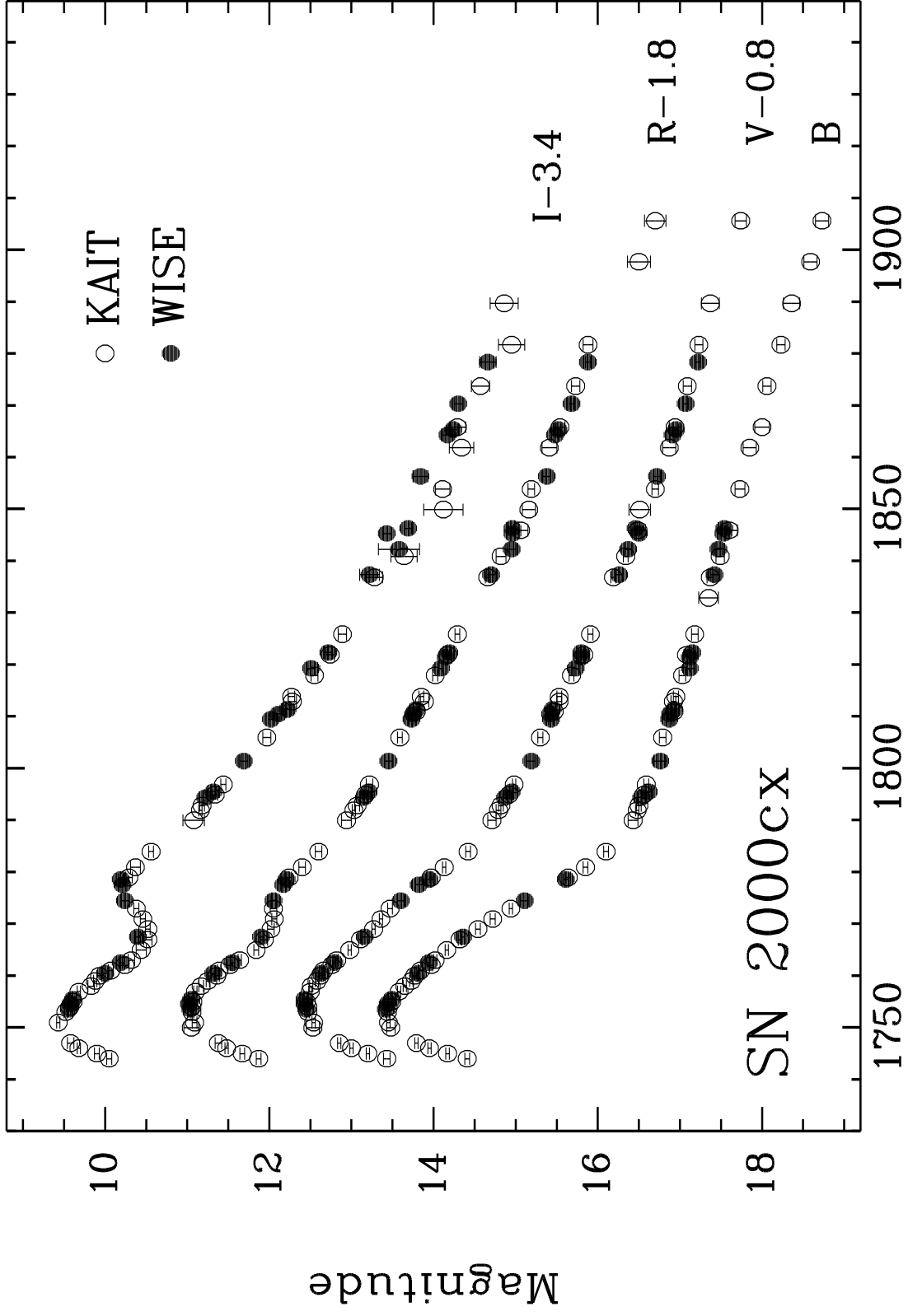
Fig. 17.— Same as in Figure 12 but for spectra at late times.

Fig. 18.— Evolution of the expansion velocity as deduced from the minima of the Fe III $\lambda 4404$, Fe III $\lambda 5129$, Fe II $\lambda 4555$, S II $\lambda 5468$, S II $\lambda \lambda 5612, 5654$, and Si II $\lambda 6355$ absorption lines for SN 2000cx (solid circles; measured from the spectra displayed in Figure 10), SN 1991T [open circles; measured from the spectra in Filippenko et al. (1992b)], and other SNe Ia. The V_{exp} derived from the Fe II $\lambda 4555$, S II $\lambda 5468$, and S II $\lambda \lambda 5612, 5654$ lines for SN 1994D are measured from the spectral series in Filippenko (1997). The expansion velocities measured from the Si II $\lambda 6355$ line are adopted from Branch et al. (1983) for SN 1981B, Phillips et al. (1987) for SN 1986G, Wells et al. (1994) for SN 1989B, Leibundgut et al. (1993) for SN 1991bg, and Patat et al. (1996) for SN 1994D.

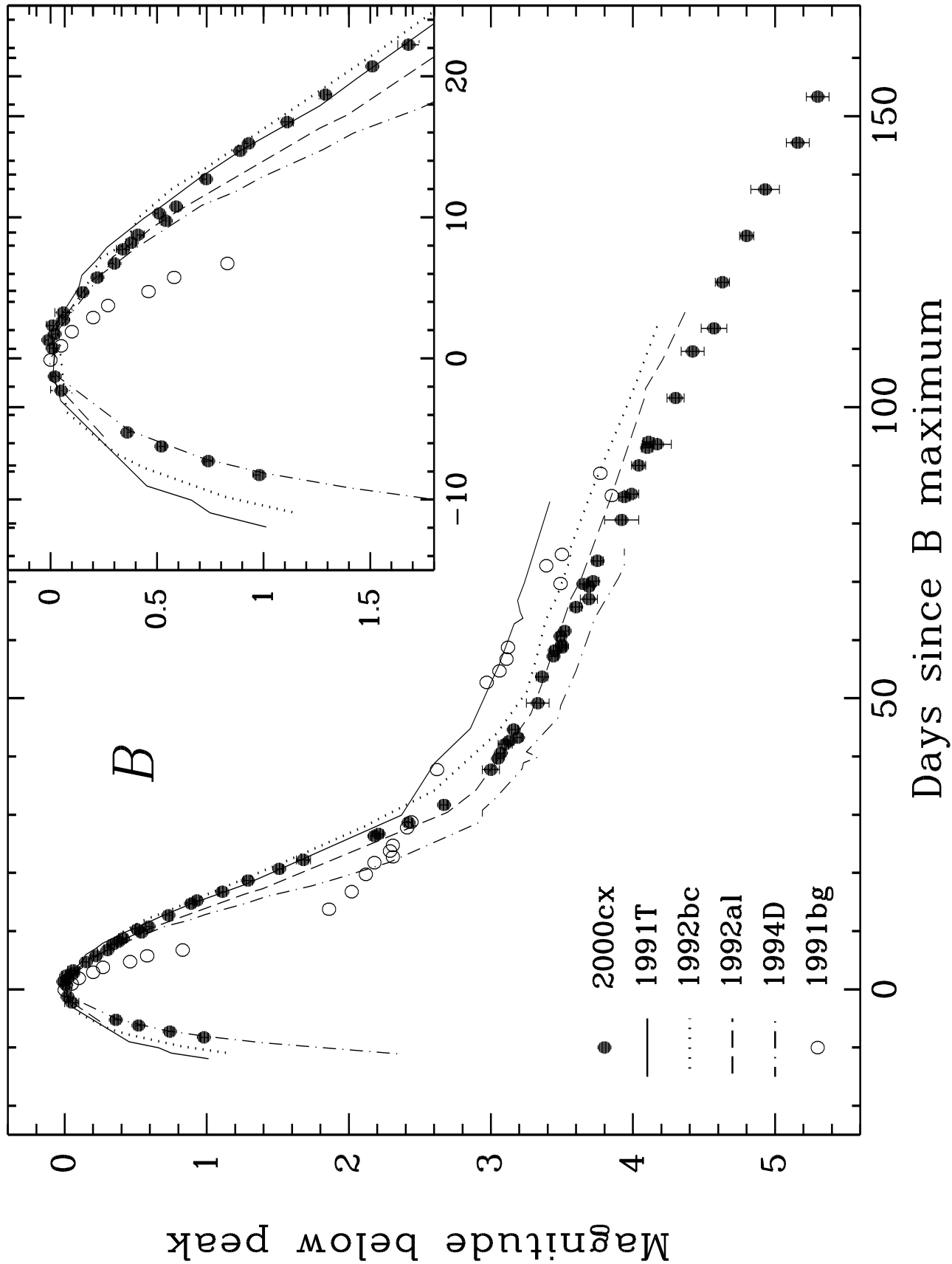
Fig. 19.— The MLCS fit (left panel) and the stretch method fit (right panel) for SN 2000cx. The MLCS fit is the worst we have ever seen. For the stretch method fit, the solid line is the fit to all the data points from $t = -8$ to 32 days, the dash-dotted line uses only the premaximum datapoints, and the dashed line for the postmaximum datapoints. The three fits give very different stretch factors.

This figure "f01.jpg" is available in "jpg" format from:

<http://arxiv.org/ps/astro-ph/0107318v1>



SN 2000cx
Julian Date - 2450000.0



Magnitude below peak

150

100

50

0

0

1

2

3

4

5

0

0.5

1

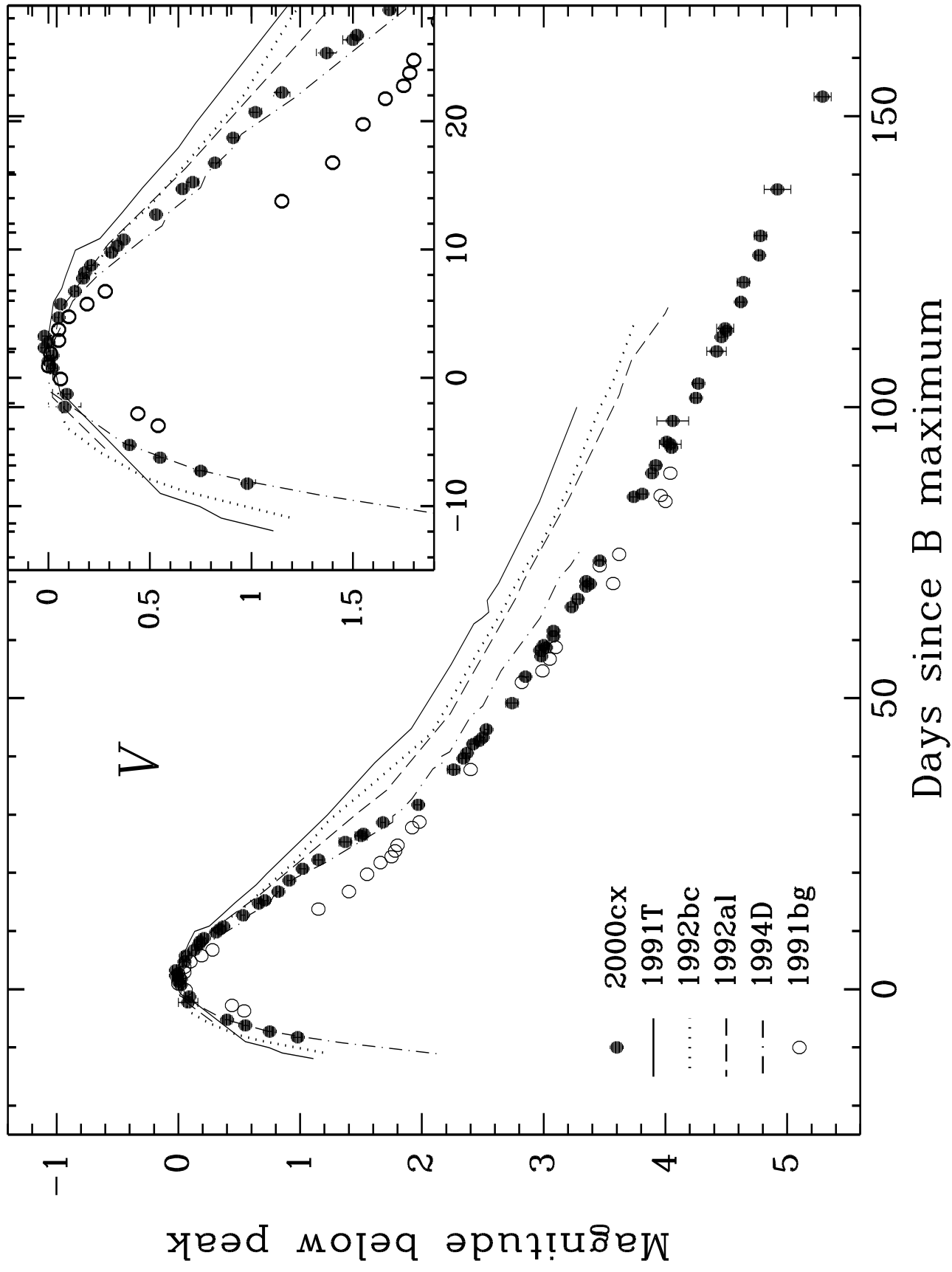
1.5

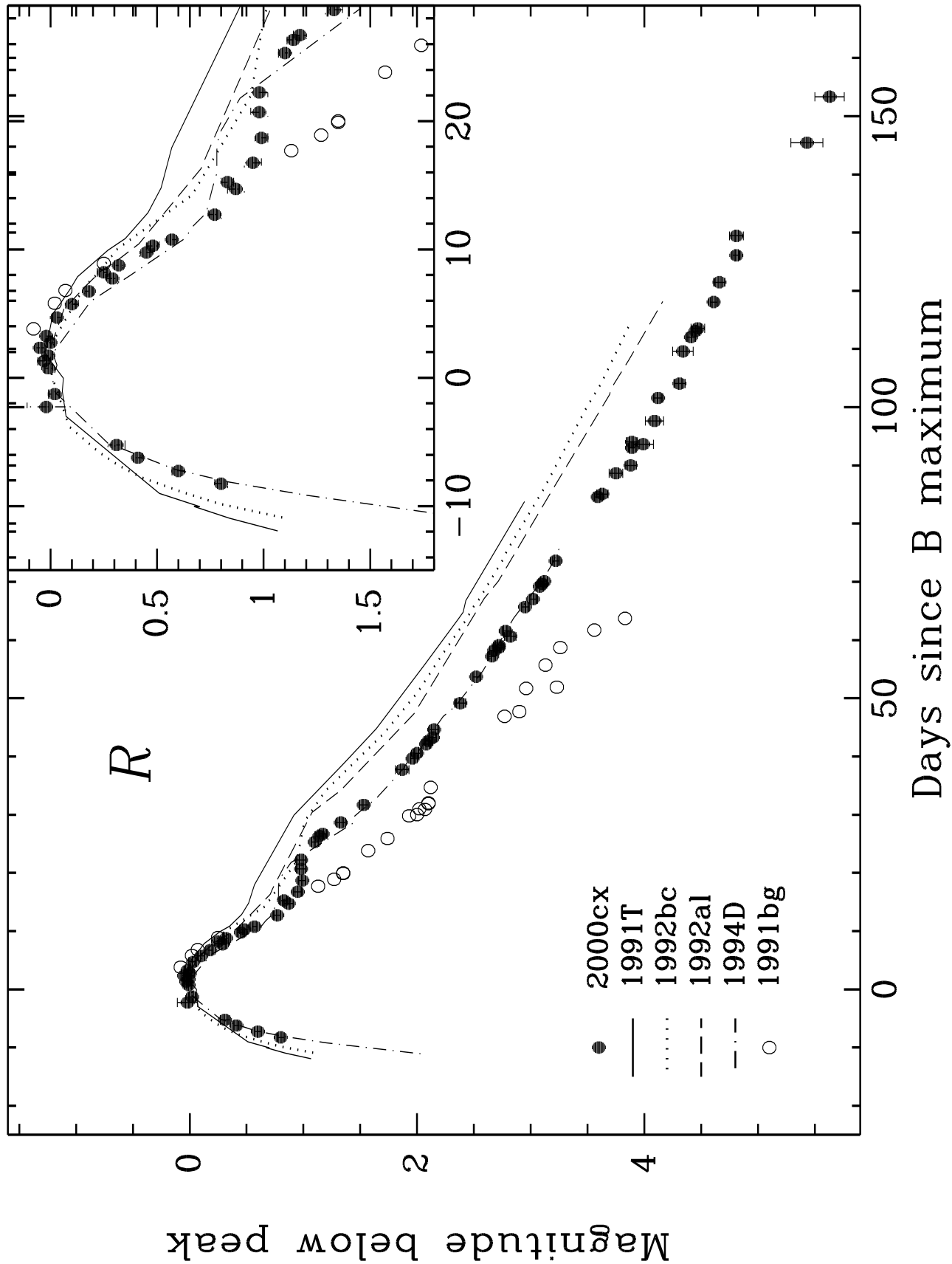
-10

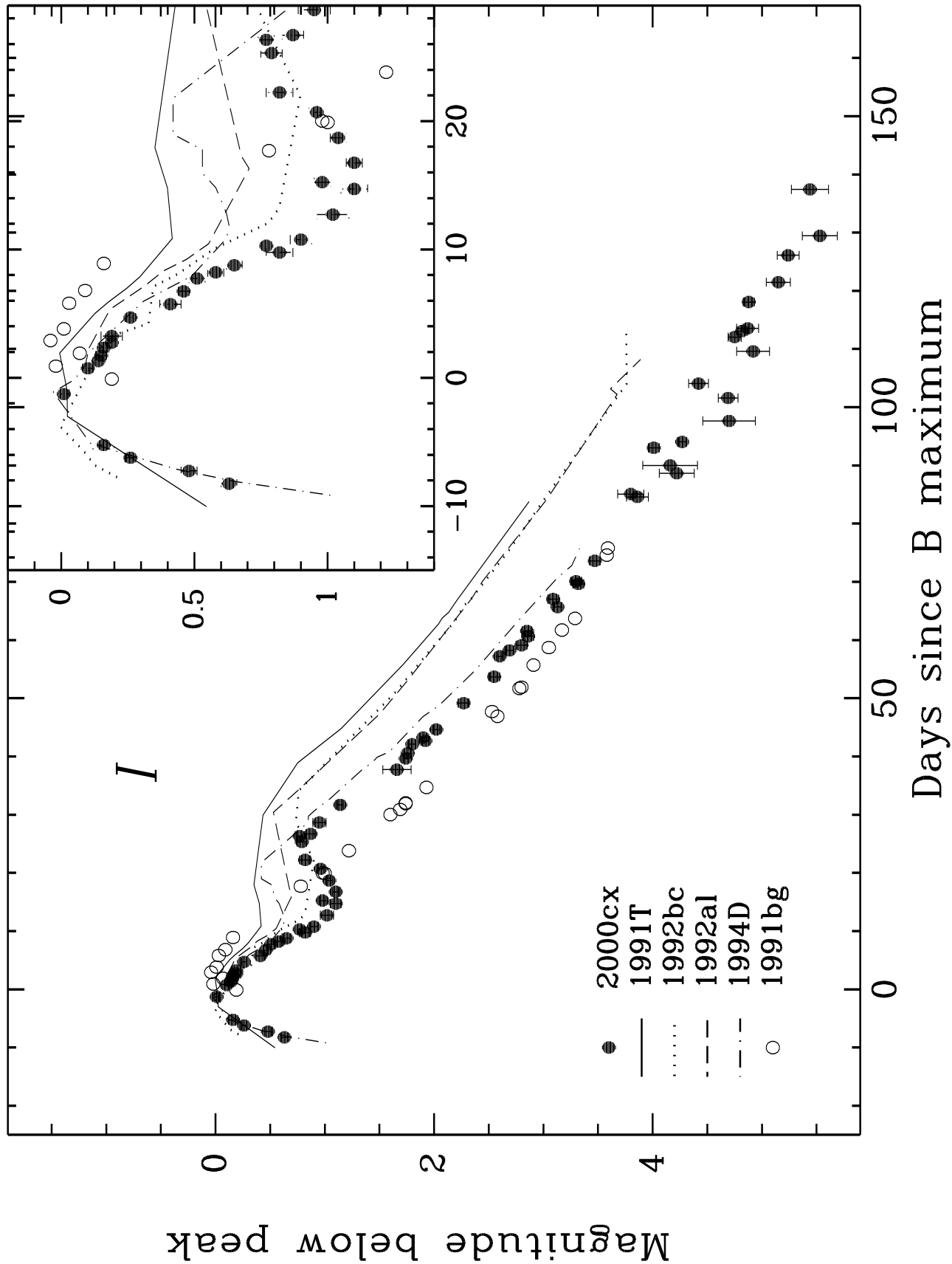
0

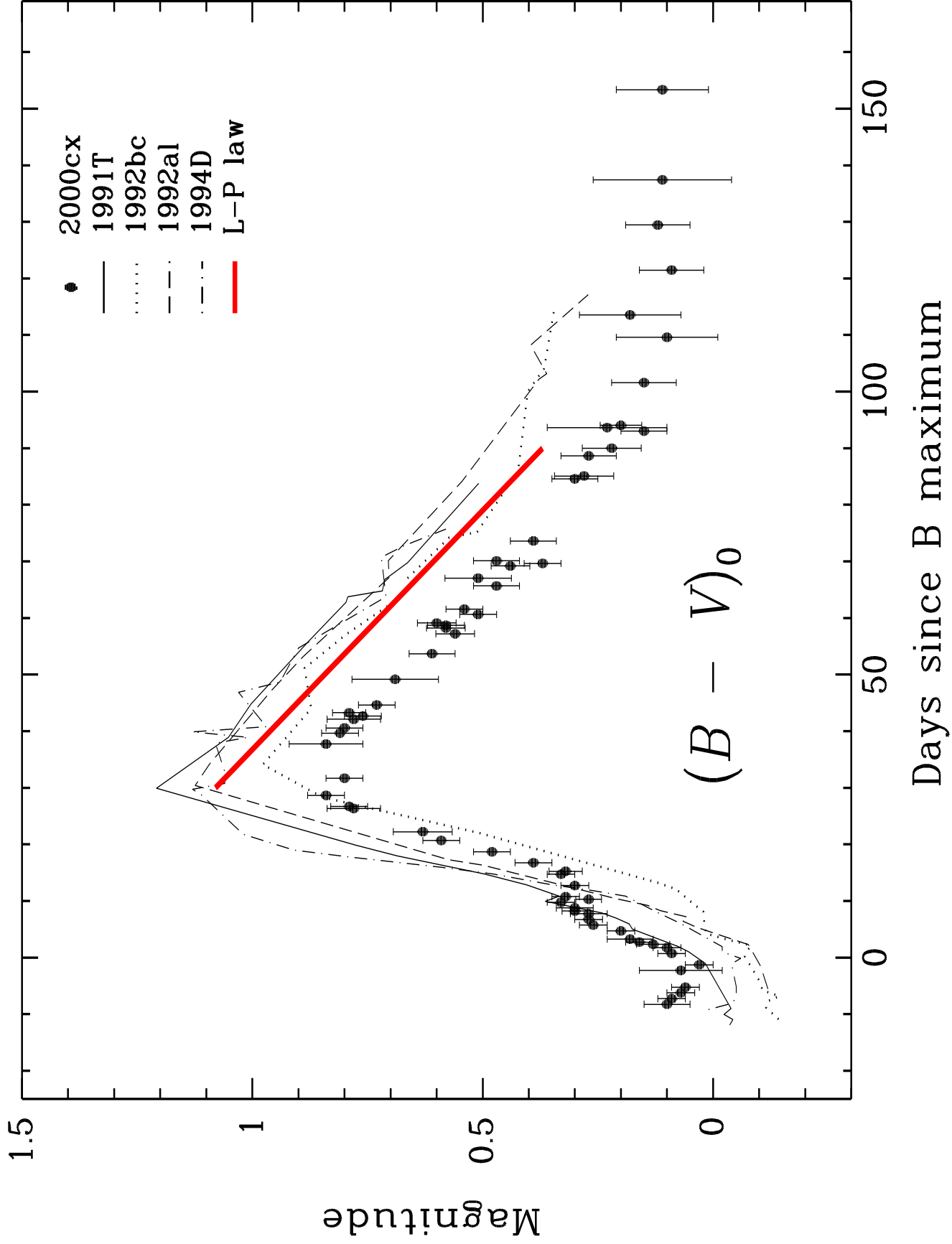
10

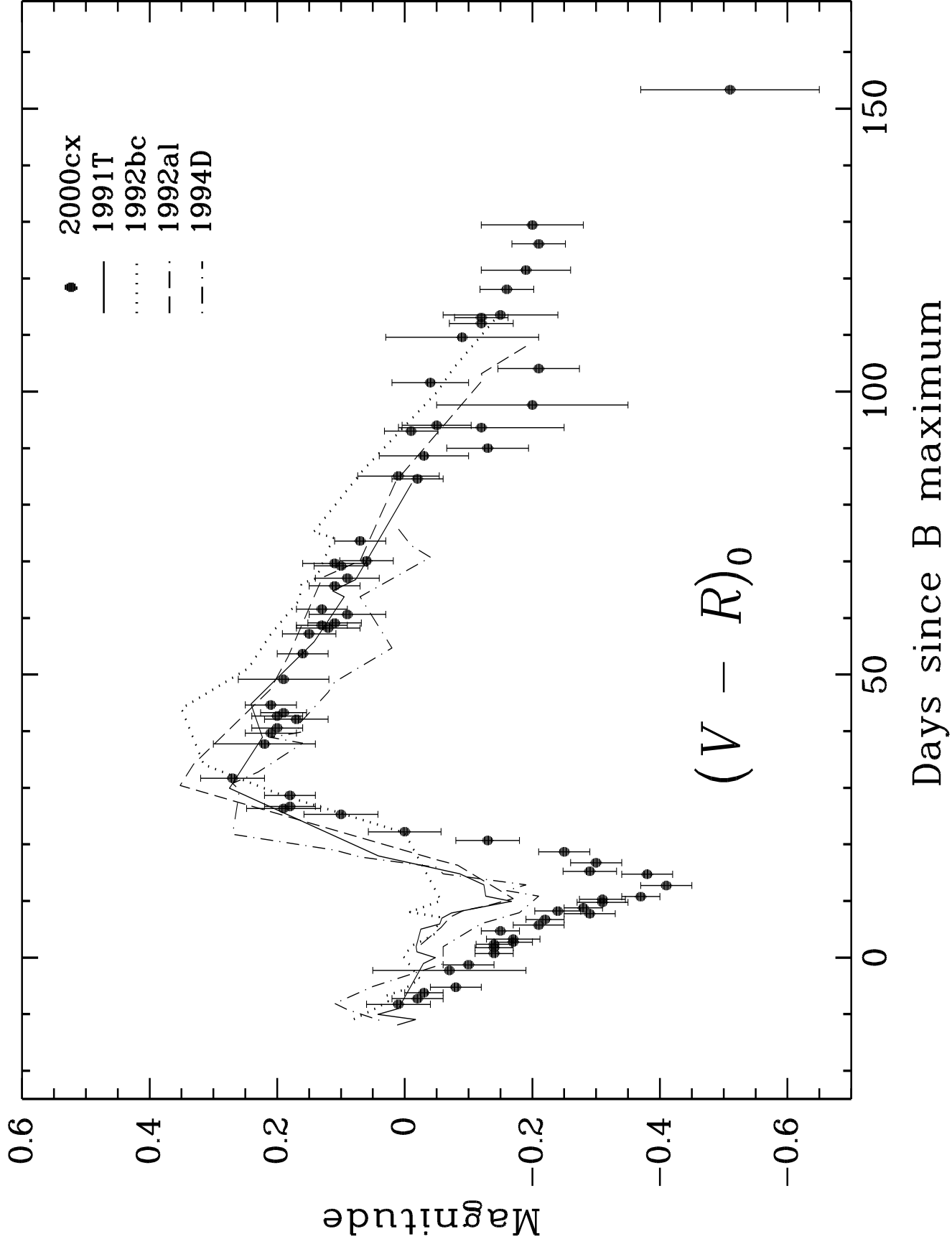
20

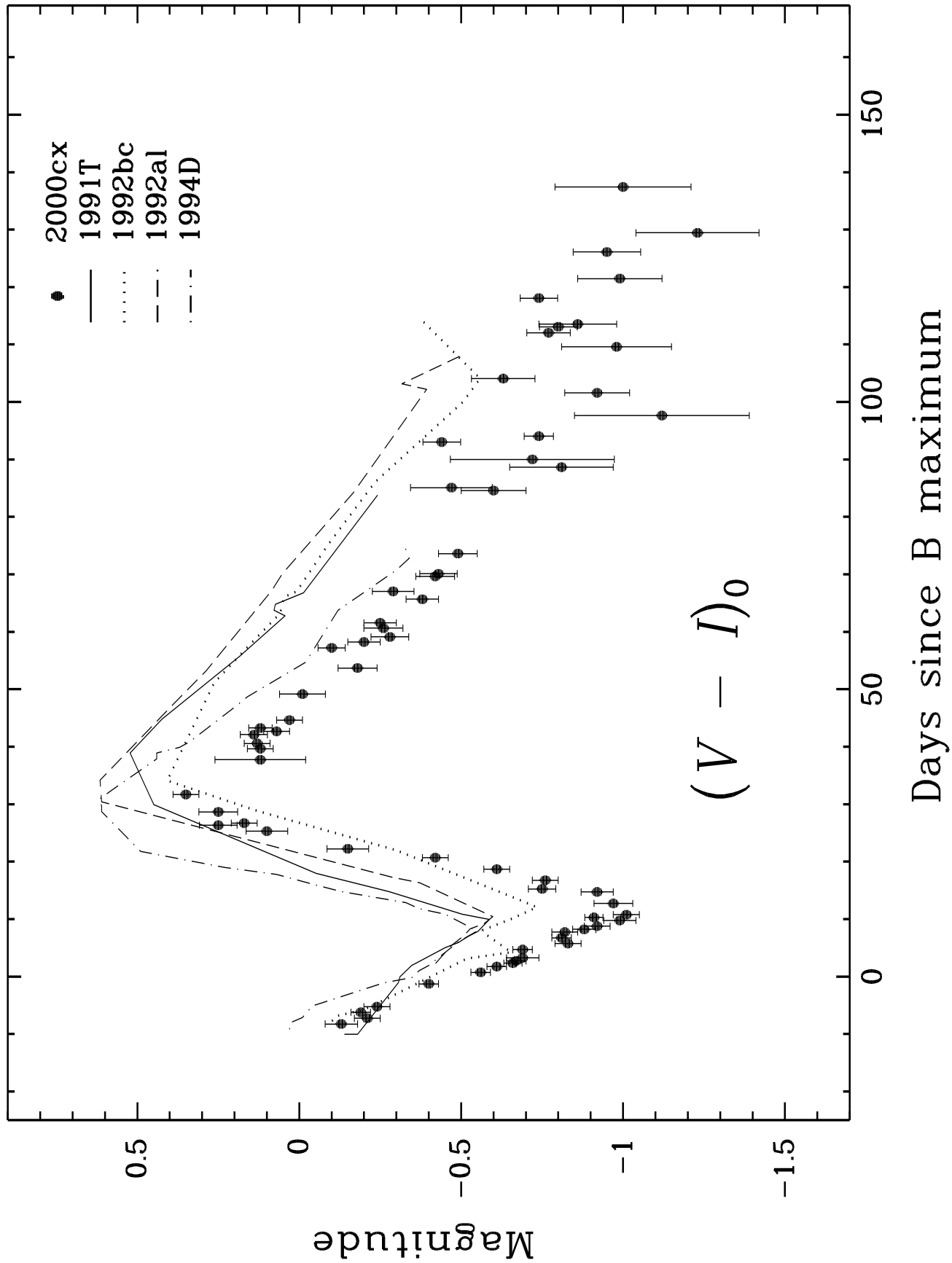












This figure "f10.jpg" is available in "jpg" format from:

<http://arxiv.org/ps/astro-ph/0107318v1>

This figure "f11.jpg" is available in "jpg" format from:

<http://arxiv.org/ps/astro-ph/0107318v1>

